

## ARTICLE



# Autoinhibitory structure of preligand association state implicates a new strategy to attain effective DR5 receptor activation

Gang Du<sup>1,6</sup>, Linlin Zhao<sup>1,2,6</sup>, Yumei Zheng<sup>1,3</sup>, Anissa Belfetmi<sup>1</sup>, Tiantian Cai<sup>1</sup>, Boying Xu<sup>2</sup>, Karen Heyninck<sup>4</sup>, Kim Van Den Heede<sup>4</sup>, Marie-Ange Buyse<sup>4</sup>, Pietro Fontana<sup>1,3</sup>, Michael Bowman<sup>5</sup>, Lih-Ling Lin<sup>5</sup>, Hao Wu<sup>1,3</sup>✉ and James Jeiwen Chou<sup>1</sup>✉

© The Author(s) under exclusive licence to Center for Excellence in Molecular Cell Science, Chinese Academy of Sciences 2022

Members of the tumor necrosis factor receptor superfamily (TNFRSF) are important therapeutic targets that can be activated to induce death of cancer cells or stimulate proliferation of immune cells. Although it has long been implicated that these receptors assemble preligand associated states that are required for dominant interference in human disease, such states have so far eluded structural characterization. Here, we find that the ectodomain of death receptor 5 (DR5-ECD), a representative member of TNFRSF, can specifically self-associate when anchored to lipid bilayer, and we report this self-association structure determined by nuclear magnetic resonance (NMR). Unexpectedly, two non-overlapping interaction interfaces are identified that could propagate to higher-order clusters. Structure-guided mutagenesis indicates that the observed preligand association structure is represented on DR5-expressing cells. The DR5 preligand association serves an autoinhibitory role as single-domain antibodies (sdAbs) that partially dissociate the preligand cluster can sensitize the receptor to its ligand TRAIL and even induce substantial receptor signaling in the absence of TRAIL. Unlike most agonistic antibodies that require multivalent binding to aggregate receptors for activation, these agonistic sdAbs are monovalent and act specifically on an oligomeric, autoinhibitory configuration of the receptor. Our data indicate that receptors such as DR5 can form structurally defined preclusters incompatible with signaling and that true agonists should disrupt the preligand cluster while converting it to signaling-productive cluster. This mechanism enhances our understanding of a long-standing question in TNFRSF signaling and suggests a new opportunity for developing agonistic molecules by targeting receptor preligand clustering.

*Cell Research* (2023) 33:131–146; <https://doi.org/10.1038/s41422-022-00755-2>

## INTRODUCTION

Most of the biologic therapeutics being developed today target transmembrane receptors of Type I/II membrane topology, which include but are not limited to immune receptors, receptor tyrosine kinases (RTKs), and death receptors. A critical step in the signaling of these receptors is ligand induced receptor dimerization, trimerization, or higher-order clustering that position the intracellular signaling domains in the optimal arrangement to initiate downstream signaling.<sup>1–9</sup> Diverse mechanisms by which a ligand induces receptor oligomerization have been discovered. For example, ligand binding to RTKs such as the EGF or ErbB receptor with 1:1 stoichiometry causes major conformational change of the ectodomain (ECD) to promote receptor dimerization.<sup>10,11</sup> A recent study on the anaplastic lymphoma kinase (ALK), also an RTK, revealed the role of ligand–membrane interaction in facilitating receptor dimerization.<sup>12</sup> For members of the tumor necrosis factor (TNF) receptor superfamily (TNFRSF), the ligands are mostly trimeric and their binding to the receptor ECD can trimerize the receptors without inducing significant conformational changes.<sup>13–16</sup>

In addition to the oligomerization directly driven by ligand binding, studies have found that regions of the receptor ECD distinct from ligand binding can self-associate to further expand the oligomerization network. One example is a cysteine-rich domain (CRD) of the Eph receptor that mediates multimerization of the ligand-stabilized dimeric unit.<sup>17</sup> Similarly, members of TNFRSF such as TNFR1, TNFR2, Fas, and GITR also contain self-associating CRDs that drive higher-order clustering of the ligand-stabilized trimeric unit.<sup>18–21</sup>

While mechanistic and structural studies have concentrated on the ligand-engaged, activated forms of the receptors, much less is known about their preligand, resting states in the context of lipid bilayer. The existence of preligand association on cell surface has been reported for several receptors using biophysical techniques. For example, it was shown with immuno-gold electron microscopy that memory T cells have more and larger T cell receptor preclusters than naïve T cells, which could explain the increased sensitivity of memory T cells to antigens.<sup>22</sup> Preligand association has also been shown for Interleukin (IL) 17 receptor (IL-17R) by

<sup>1</sup>Department of Biological Chemistry and Molecular Pharmacology, Harvard Medical School, Boston, MA, USA. <sup>2</sup>Tongji University Cancer Center, Shanghai Tenth People's Hospital, School of Medicine, Tongji University, Shanghai, China. <sup>3</sup>Program in Cellular and Molecular Medicine, Boston Children's Hospital, Boston, MA, USA. <sup>4</sup>Sanofi, Technologiepark 21, Zwijnaarde, Belgium. <sup>5</sup>Checkpoint Immunology, Immunology & Inflammation, Sanofi, Cambridge, MA, USA. <sup>6</sup>These authors contributed equally: Gang Du, Linlin Zhao.

✉email: [wu@crystal.harvard.edu](mailto:wu@crystal.harvard.edu); [james\\_chou@hms.harvard.edu](mailto:james_chou@hms.harvard.edu)

Received: 18 September 2022 Accepted: 15 November 2022

Published online: 6 January 2023

fluorescence resonance energy transfer (FRET) measurements, and in that case, ligand binding to IL-17R caused markedly reduced FRET efficiency, suggesting that the preligand and ligand-induced receptor associations are structurally very different.<sup>23</sup>

In particular, preligand association mediated by receptor ECD has been most extensively tested for receptors in the TNFRSF, which are therapeutic targets that can be activated to induce death of some cancer cells or stimulate proliferation of immune cells.<sup>24–27</sup> These receptors are typical type-I transmembrane proteins comprising a ligand-binding ECD, a transmembrane domain (TMD), and an intracellular region that interacts with signaling adaptor such as the Fas-associated death domain, the TNFR1-associated death domain or the TNFR-associated factors.<sup>28–30</sup> Measurements of FRET between receptor variants fused to either cyan or yellow fluorescent protein (CFP or YFP) showed that the ECD mediates preligand multimerization of TNFR1 and Fas on the cell surface<sup>19,21</sup> and these observations have later been independently validated by super-resolution light microscopy.<sup>31,32</sup> The oligomeric state of preligand association has been debated between dimeric<sup>30</sup> and trimeric<sup>33</sup> although there was not compelling evidence for either form. Crystallographic study of solubilized ECD of TNFR1 in the absence of ligand showed two dimeric interfaces in the crystal, resulting in both parallel and antiparallel dimers.<sup>20</sup> In the crystal structure of another TNFRSF member, 4-1BB, the ECD shows an antiparallel arrangement.<sup>34</sup> Since the above receptor ECDs are monomeric in solution, it remains unclear whether these interactions were the results of crystal packing.

In addition to ECD-mediated preligand interaction, the TMDs of some of the TNFRs such as Fas, TNFR1, and p75(NTR) have the intrinsic propensity of oligomerizing in membrane,<sup>32,33,35,36</sup> which further complicates the situation with potential ECD-TMD coupling relevant for receptor activation. For example, the TMD of DR5 can form a dimer-trimer interaction network in the membrane that is essential for ligand-induced receptor signaling.<sup>37</sup> Proteolytic removal of the ECD can activate DR5 to the same extent as its endogenous ligand TRAIL, and this striking effect has been observed for other TNFRSF members such as OX40 and TNFR2.<sup>37</sup> These results suggest that the ECD should form a defined oligomeric complex on the membrane that prohibits TMD-mediated receptor activation in the absence of ligand.

This study aims to address the structural and functional properties of receptor preligand association by using DR5 as a study case. We developed a sample system in which the ECD of DR5, designated DR5-ECD, is anchored to bicelles that closely mimic a lipid disc. Bicelle-anchoring allowed the ECD to cluster from otherwise monomeric state in solution. We then performed structural analysis by nuclear magnetic resonance (NMR) and found that DR5-ECD indeed oligomerizes with two non-overlapping interfaces when anchored to a lipid bilayer and such interactions also exist on the cell surface as shown by live cell imaging. To test the functional role of the preligand structure, we identified single-domain antibodies (sdAbs) that specifically disrupt DR5 preligand association and found that these monovalent molecules can induce very significant signaling even in the absence of ligand. Our studies provide direct structural evidence of receptor preligand association while demonstrating the potential for developing new agonists that selectively target these states.

## RESULTS

### DR5-ECD is largely monomeric in solution but oligomerizes on liposomes

To characterize preligand association of DR5-ECD, it is critical to develop a sample system amenable to biochemical and biophysical analyses. We expressed the ECD (residues 56–182) of human DR5 with a C-terminal polyhistidine tag (His-tag) in yeast (*Pichia pastoris*) (Fig. 1a), which is an expression system suitable for cysteine-rich proteins but also compatible with isotope labeling

for NMR studies.<sup>38</sup> The purified DR5-ECD in solution is, however, monomeric as indicated by size-exclusion chromatography with multi-angle light scattering (SEC-MALS, Supplementary information, Fig. S1a, b), and this is consistent with previous observations of monomeric ECDs of other receptors of TNFRSF that have delayed our recognition of preligand association. To reconstitute the problem more accurately, we anchored the DR5-ECD to a lipid bilayer blended with Ni-NTA lipids (DGS-NTA) via interaction between its C-terminal His-tag and Ni-NTA (Fig. 1b). Anchoring the ECD onto a two-dimensional bilayer pays for the rotational entropy cost, facilitating the protein to self-associate. We first tested self-association of DR5-ECD on DMPC liposome blended with DGS-NTA (at 1:10 DGS-NTA:DMPC ratio). Cy3/Cy5 was labeled at residue 77 (mutated to Cys), which is an unstructured residue near the first CRD (CRD1), for generating FRET readout of self-association. As expected, mixing 1:1 ratio of Cy3-DR5-ECD and Cy5-DR5-ECD (10  $\mu$ M total protein concentration) in solution did not generate stronger FRET than mixing the two dyes, confirming that DR5-ECD is monomeric in solution. In the presence of liposomes, however, strong FRET was observed, and further addition of TRAIL reduced FRET (Fig. 1c). TRAIL binding trimerizes DR5-ECD and should increase FRET if liposome-anchored ECDs alone are monomeric. The fact that the FRET is lower in the presence of TRAIL suggests that the CRD1 domains of the self-associated DR5-ECD in the preligand state are closer than in the TRAIL-bound state.

### NMR and biochemical characterization of bicelle-anchored DR5-ECD

Based on the liposome anchoring approach, we anchored DR5-ECD to DMPC-DH<sub>7</sub>PC bicelles with [lipid]/[detergent] ratio ( $q$ ) of  $\sim 0.5$ . DH<sub>7</sub>PC was used instead of the commonly used DH<sub>6</sub>PC to minimize free detergent, as it has  $\sim 10$  times lower critical micelle concentration than DH<sub>6</sub>PC. In the absence of bicelles, (<sup>15</sup>N, <sup>2</sup>H)-labeled DR5-ECD expressed by yeast yielded high quality spectrum with excellent peak homogeneity and chemical shift dispersion (Fig. 1d), consistent with monomeric DR5-ECD (15.5 kDa) in solution. Upon mixing with bicelles at 30 °C, the spectrum became more heterogeneous due to binding to the bicelles, but in addition, a subset of peaks gradually moved over time (Fig. 1e; top) until the protein began to precipitate after  $\sim 7$  days. Chemical crosslinking of the NMR sample showed increasing population of oligomers at longer time points (Supplementary information, Fig. S1c), suggesting that the specific and time-dependent chemical shift changes were due to continued clustering of the protein on bicelles. Moreover, these shifted peaks were retrospectively found to come from residues within the interaction interfaces (see below). The uncontrolled clustering was problematic for structural characterization, which prompted a systematic screening of parameters including protein concentration, bicelle  $q$ , and temperature. Fortunately, we found that at 37 °C and 0.5 mM total DR5-ECD concentration, higher-order clustering is much slower (Fig. 1e; bottom), providing a window of 4–6 days to collect NMR data for structural characterization.

### Bicelle-anchored DR5-ECD shows two non-overlapping self-association interfaces

We first performed thorough analysis of intramolecular nuclear Overhauser effects (NOEs) of bicelle-anchored DR5-ECD. The NOE-derived contact matrix is in strong agreement with those of the crystal structure of TRAIL- or antibody- bound DR5-ECD (Supplementary information, Fig. S1d),<sup>16,39</sup> indicating that ligand binding does not induce significant conformational change of DR5-ECD, just as TNF $\beta$  binding does not significantly perturb the structure of TNFR1-ECD.<sup>15,20</sup> We next attempted to detect intermolecular NOEs due to protein self-association by using an isotopically mixed sample containing 1:1 mixture of (<sup>15</sup>N, <sup>2</sup>H)-labeled DR5-ECD and <sup>13</sup>C-labeled DR5-ECD, but cluster of DR5-ECD on bicelle

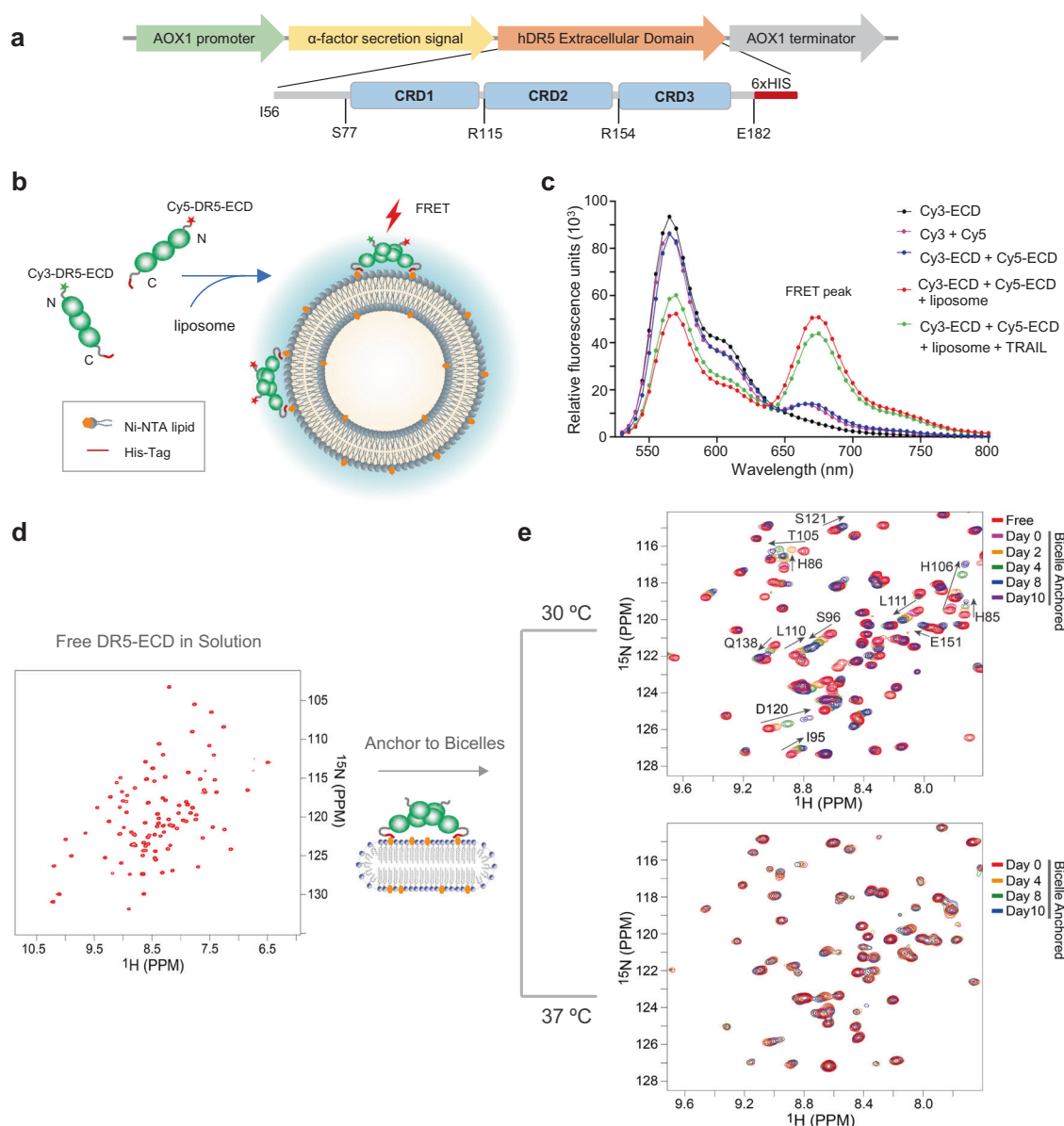


**Fig. 1 FRET and NMR characterization of DR5-ECD anchored to lipid bilayer.** **a** The ECD construct of human DR5 for yeast expression and spectroscopic studies. **b** Schematic illustration of a FRET assay for quantifying ECD self-association when anchored to liposomes. Cy3/Cy5 is labeled at residue 77 of the S77C mutant of DR5-ECD. **c** FRET spectra recorded by excitation of Cy3 at 510 nm and emission from 520–800 nm, showing strong appearance of Cy5 emission due to Cy3–Cy5 FRET when the proteins are anchored to liposomes. The spectrum color definitions are: black, 5  $\mu\text{M}$  Cy3-ECD in solution; purple, mixture of 5  $\mu\text{M}$  Cy3 and 5  $\mu\text{M}$  Cy5 dyes; blue, mixture of 5  $\mu\text{M}$  Cy3-ECD and 5  $\mu\text{M}$  Cy5-ECD in solution; red, mixture of 5  $\mu\text{M}$  Cy3-ECD and 5  $\mu\text{M}$  Cy5-ECD in the presence of liposome; green, mixture of 5  $\mu\text{M}$  Cy3-ECD and 5  $\mu\text{M}$  Cy5-ECD in the presence of liposome and 10  $\mu\text{M}$  of TRAIL. **d** The  $^1\text{H}$ - $^{15}\text{N}$  TROSY-HSQC spectrum of ( $^{15}\text{N}$ ,  $^2\text{H}$ )-labeled DR5-ECD in solution recorded at 30 °C. **e** Spectral changes of DR5-ECD over a course of 10 days after anchoring to DMPC-DH<sub>7</sub>PC bicelles ( $q = 0.5$ ) at 30 °C (top) and 37 °C (bottom).

was too large to apply the sensitivity-costly  $J_{\text{CH}}$ -modulated experiment for selecting intermolecular NOEs.<sup>40</sup> We instead used a strategy that involves (1) splitting a ( $^{15}\text{N}$ ,  $^2\text{H}$ )-labeled sample to two halves, one mixed with  $^{13}\text{C}$ -labeled DR5-ECD at 1:1 ratio and the other not mixed, and (2) recording identical  $^{15}\text{N}$ -edited NOESY-TROSY spectra (which is highly sensitive) for the two samples. Obvious intermolecular NOEs could be identified by direct comparison between the mixed and unmixed spectra (Supplementary information, Fig. S2a). Analysis of intermolecular NOEs indicated two distinct interaction interfaces, which informed subsequent assignment of self-consistent intermolecular NOEs from other regular NOE experiments (Supplementary information, Fig. S2b).

### Structural details of the two non-competing preligand associations

Since intermolecular NOEs indicated the presence of two non-overlapping self-interacting interfaces that can in principle form a variety of oligomers, a unique oligomeric state may not exist in the sample. Thus, for structure calculation, a trimer template was used as it is the smallest oligomer that can cover intermolecular NOEs from both interfaces. We first refined the monomer structure against all intramolecular NOEs. We first used intramolecular NOEs to refine the monomer structure, which was then used to calculate the trimer structure containing both interfaces by applying a total of 61 intermolecular distance restraints (37 for Interface 1; 24 for Interface 2) in rigid-body restrained dynamics

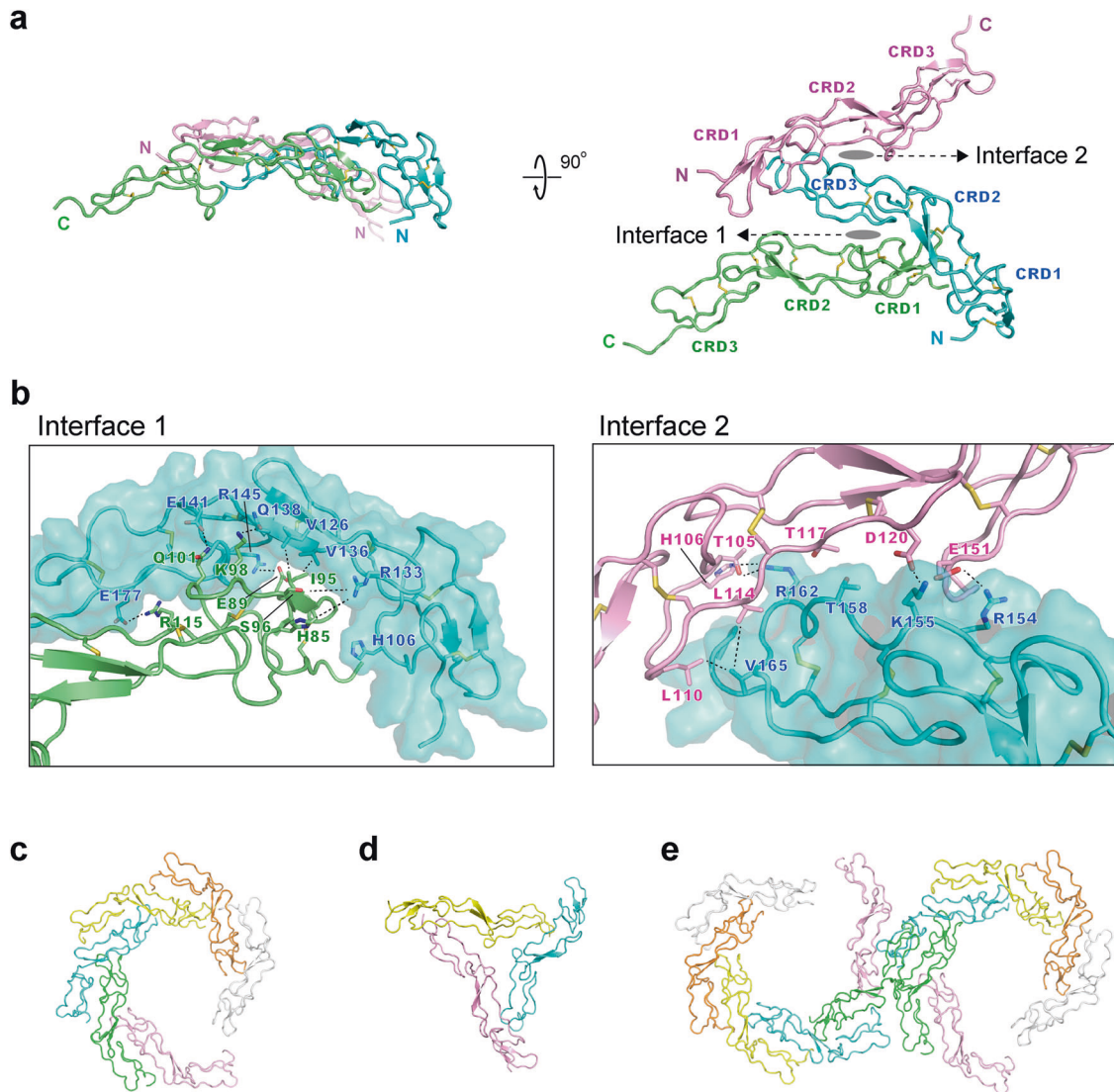


**Fig. 2 Structures of DR5-ECD preligand associations on bicelles.** **a** Cartoon representation of a trimeric assembly of bicelle-anchored DR5-ECD that contains the two non-overlapping interaction interfaces. **b** Detailed views of Interfaces 1 and 2 for highlighting residues that appear to participate in hydrophilic (electrostatic or salt bridge) or hydrophobic interactions between the neighboring monomers. **c–e** Possible higher-order assemblies by replicating Interface 1 (**c**), replicating Interface 2 (**d**), and combining Interfaces 1 and 2 (**e**).

(Fig. 2a; Supplementary information, Fig. S2c, d and Table S1). We note that the calculated structure of the trimeric complex, although a real possibility, should not be interpreted as the only oligomeric state of the membrane-anchored DR5-ECD. The calculated trimeric complex in Fig. 2a is for showing the two non-overlapping interaction interfaces in one structural model.

Interface 1 can be characterized by insertion of CRD1 of one monomer into the arch of the neighboring monomer (Fig. 2b; left). Based on the structure, key inter-monomer interactions appear to be S96–R133, E89–R145, I95–V136, K98–Q138, and R115–E177. Interface 2 is characterized by association of CRD2 and CRD3 of one monomer with CRD2 and CRD1 of another monomer, respectively, involving completely different regions of the protein. In this case, key inter-monomer interactions appear to be R154–E151, K155–D120, and V165–L110/L114 (Fig. 2b; right). It is interesting to mention that some of these residues in the two interaction interfaces, e.g., H85, I95, S96, L110, L111, D120, S121, Q138, and E151, happen to correspond to peaks that have shifted the most over time at 30 °C (Fig. 1e), suggesting that the two modes of interactions are weak and dynamic but became more stable over time due to higher cooperativity as the cluster grew

larger. On that note, the majority of the interactions appear to be salt bridges that could be destabilized by high thermal energy, explaining why cluster-driven NMR spectral change is much slower at 37 °C.

#### Possible higher-order assemblies based on the two interactions

Since the two interaction interfaces of bicelle-anchored DR5-ECD are on opposite sides of the protein (Fig. 2a), higher-order clusters can be envisaged by replicating the interfaces without causing steric collision with either protein or lipid bilayer. Interface 1 can, in principle, replicate and propagate to a ring-like structure with CRD1s inside and CRD3s on the periphery (Fig. 2c). Since the two neighboring ECDs are orientated at ~50° relative to each other, ~7 monomers would be needed to close the ring. The other interface (Interface 2) involves a head-to-tail interaction that position the neighboring ECDs at ~120° relative to each other; this interaction alone can, in principle, form a trimer (Fig. 2d). Combining the two interactions could assemble even larger clusters in which Interaction 1 assembles the ring structure and Interaction 2 stitches the rings together to form multimer of rings (Fig. 2e).



The above interfaces were determined exclusively using intermolecular NOEs, which can only detect short  $^1\text{H}$ - $^1\text{H}$  distances ( $<5$  Å). We also examined the preligand association by measuring intermolecular paramagnetic relaxation enhancement (PRE), which can probe longer distances ( $<25$  Å)<sup>41,42</sup>. In this experiment, we used ( $^{15}\text{N}$ ,  $^2\text{H}$ )-labeled ECD for NMR readout and non-isotope labeled ECD with nitroxide spin label conjugated at residue position 77 (SL77) or 183 (SL183) for introducing PRE (Supplementary information, Fig. S3a). Due to the flexible linker of the spin label and its unknown positional distribution, PREs are not quantitative measure of distances and were thus not included in structure determination. They are nevertheless good measurables for providing independent, qualitative validation of the oligomer structures derived from NOEs. The strong intermolecular PREs overall agree with the two interfaces, but not all strong PREs can be explained by the trimer model in Fig. 2. For example, SL77 near CRD1 of monomer 2 generated strong PREs in CRD2 of monomer 3, as expected from the Interface 1 structure, but also generated PREs in CRD3 far from the spin label (Supplementary information, Fig. S3b, c). By expanding the trimer model by adding additional monomers via Interfaces 1, we found that spin labels from monomer 1 can account for the PREs in CRD3. Another example is that SL183 of monomer 8 generated strong PREs in CRD2 of monomer 9 but could not account for PREs in CRD1 (Supplementary information, Fig. S3b, d). In this case, including monomer 7 via Interface 1 and monomer 3 via Interface 2 could explain the additional PREs. Collectively, the intermolecular PREs suggest that higher than dimeric assemblies represented within the hypothetical cluster in Fig. 2e are randomly distributed in the NMR sample.

#### DR5-ECD lies flat on lipid bilayer, partially concealing its TRAIL binding site

In addition to protein self-association, an important aspect of receptor preligand structure is how receptors are positioned on the cell membrane. We addressed this question by measuring PRE using two different lipophilic paramagnetic probes. In the first experiment, we measured PRE caused by the partitioning of N-tempyl palmitamide (N-TP), which places the nitroxide in the headgroup region of the lipid bilayer part of the bicelles (Fig. 3a). We found that the side of CRD1 with residues 105–115 showed the strongest PRE (Fig. 3a). In another experiment, we performed the paramagnetic probe titration (PPT) analysis<sup>40,43,44</sup> using 5-DOXYL-stearic acid (5-DSA) as the paramagnetic probe, which is fatty acid with a nitroxide at the C5 position (Fig. 3b). Titrating 5-DSA to bicelle-anchored DR5-ECD generated dose-dependent decay of NMR signals (Fig. 3c). The titration data were fitted to Eq. 1 (Materials and Methods) to determine the PRE amplitude ( $\text{PRE}_{\text{amp}}$ ), with larger value of  $\text{PRE}_{\text{amp}}$  meaning closer to lipid bilayer (Fig. 3d). The PPT results also indicate that the N-terminal region is in contact with the bicelle surface although only the C-terminus is physically anchored to the bicelle. The above two experiments together show that in contrast to the general depiction of cell surface receptors “standing up” on the membrane, DR5-ECD rests flat on lipid bilayer in a specific posture, with its TRAIL binding site partially buried (Fig. 3e).

#### Disrupting DR5 preligand association sensitizes the receptor to TRAIL

Partial seclusion of TRAIL binding site by DR5 preligand clustering (Fig. 3e) suggests that disruption or weakening of DR5-ECD self-association should facilitate TRAIL binding. To test this hypothesis, we examined five anti-DR5 NANOBODY<sup>®</sup> compounds,<sup>45</sup> designated NB1–NB5, for their ability to disrupt the preligand association using the liposome-based FRET assay (Fig. 1b). For convenience, the names “NANOBODY” compound and “sdAb” are used interchangeably hereafter. All five sdAbs have very high binding affinity for DR5-ECD ( $K_D < 10$  nM; Table 1), but only NB1

and NB5 caused significant drop in FRET (Fig. 4a), indicating disruption (at least partial) of the liposome-anchored DR5-ECD clusters. We then used stable HEK293T cells expressing DR5 for testing functional properties of these sdAbs. Two standard TRAIL dose-response activation profiles were established using two independent readouts, caspase-8 activity and cell viability (Fig. 4b), which showed that receptor signaling reached saturation at  $\sim 200$  ng/mL TRAIL and provided the magnitude of ligand-induced activity for normalizing all subsequent activity measurements.

Based on the caspase-8 activity readout, dose-response profiles for NB1–NB5 were generated using the same batch of cells in the presence of 50 ng/mL TRAIL, a concentration that could only achieve  $\sim 18\%$  of full activation by TRAIL. NB3 and NB4 did not show any activity, as was the case of a negative-control sdAb (NB0) that does not bind DR5-ECD (Fig. 4c). NB1 and NB5 exhibited the strongest agonistic effect by increasing activity from  $\sim 18\%$  to  $\sim 63\%$  (Fig. 4c), consistent with their ability to disrupt the preligand association (Fig. 4a). NB2 also augmented activity to  $\sim 46\%$ , although it showed weak interference of preligand association, similar to NB3 that showed no agonistic function. This is because NB3 blocks TRAIL binding whereas NB2 does not (Table 1). The same dose-response measurements were performed using cell viability as readout in the presence of 25 ng/mL TRAIL, and the results matched closely to that derived from caspase-8 activity (Fig. 4d). To understand how NB1 or NB5 can disrupt preligand association, we performed epitope mapping by measuring NMR chemical shift perturbation of DR5-ECD caused by NB1 binding (Supplementary information, Fig. S4a, b). We found that NB1 binding site on DR5-ECD overlaps strongly with Interface 1 of the preligand association but not with the TRAIL binding site (Fig. 4e), consistent with the ability of DR5-ECD to form ternary complex with TRAIL and NB1 (Supplementary information, Fig. S4c). The above data suggest that a sdAb that can disrupt or weaken preligand association has the function of sensitizing DR5 to its endogenous ligand if it does not block ligand binding. This is consistent with a mechanism in which the TRAIL binding site is buried in the preligand cluster, and loosening the cluster, even partially, can increase exposure of the site, triggering activation at much lower ligand concentration than normally required.

#### DR5 activation by sdAbs in the absence of TRAIL

We next investigated agonistic potential of NB1–NB5 independent of ligand using the same stable HEK293T cells expressing DR5. In the absence of TRAIL, NB1 and NB5 individually could only induce modest activity ( $\sim 20\%$ ) at high concentration (Fig. 5a; Supplementary information, Fig. S5a, b). The weak agonistic function could be attributed to insufficient disruption of the preligand association. We then explored possible synergy between different sdAbs for further dissociating the preligand cluster. We examined all combinations of two sdAbs out of the five in the liposome-based FRET assay. Indeed, some of the combinations further disrupted preligand association. For example, NB5 alone decreased FRET by 24% and NB3 alone did not cause significant FRET reduction (Fig. 4a). However, when combined, the two further reduced FRET by 46% (Fig. 5b). Similarly, NB1 also showed substantially stronger disruption of preligand association when combined with NB3 (Fig. 5b). The above two synergistic combinations exhibited even stronger synergy in receptor activation assay, with the (NB5, NB3) combination improving the activity to  $\sim 40\%$  and the (NB1, NB3) combination improving the activity to  $\sim 60\%$  of saturated activation by TRAIL (Fig. 5c, d; Supplementary information, Fig. S5c). We have confirmed that DR5-ECD can bind simultaneously to both NB1 and NB3 (Supplementary information, Fig. S5d), indicating that they bind to different sites on DR5-ECD. Comparison between FRET reduction and receptor activation data from all single and duo sdAbs showed a positive correlation

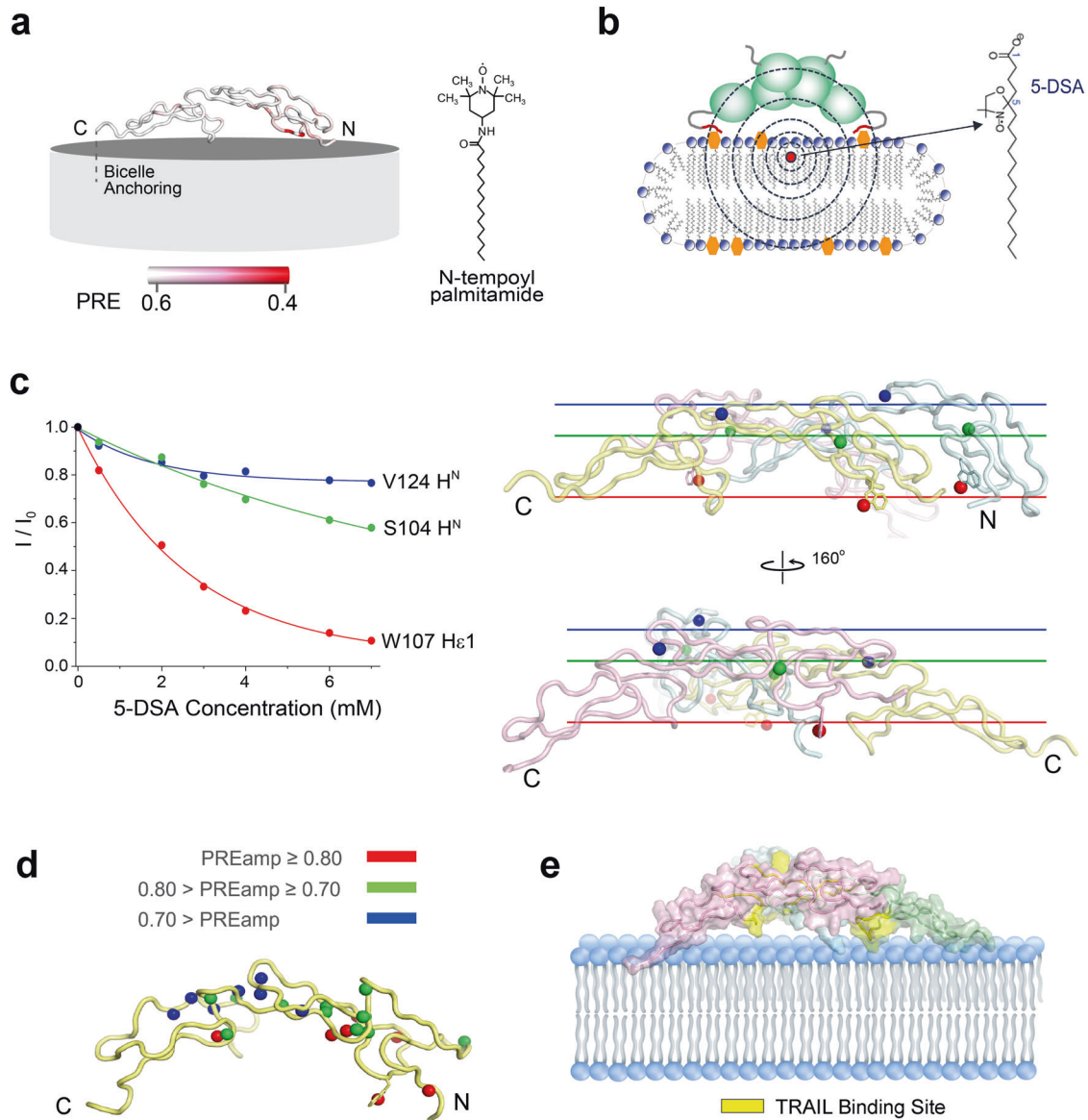


**Fig. 3 Characterization of the resting position of DR5-ECD on lipid bilayer.** **a** Mapping of residue-specific PRE induced by 2 mM N-TP onto the DR5-ECD monomer structure with the color spectrum of PRE values defined in the Figure. PRE is defined as the ratio of peak height of bicelle-anchored DR5-ECD in the presence ( $I$ ) and absence ( $I_0$ ) of N-TP. **b** Schematic illustration of the use of the lipophilic paramagnetic probe, 5-DOXYL-stearic acid (5-DSA), for determining the resting position of the DR5-ECD cluster on bicelles. **c** Paramagnetic probe titration using the lipophilic probe 5-DSA for identifying the side of the DR5-ECD cluster that faces the bicelle. Example signal decay curves (left panel) are shown for W107, S104, and V124, which mark three different elevations (right panel) from the bicelle surface, respectively. The colors of the spheres in the structure match that of the plots in representing the residue numbers. The curve fitting is described in Materials and Methods. **d** Mapping of residue-specific  $PRE_{amp}$  (determined by good fitting to Eq. 1 in Materials and Methods) onto the DR5-ECD monomer structure with the color spectrum of  $PRE_{amp}$  values defined in the figure. Larger  $PRE_{amp}$  means closer to the bicelle. **e** Positioning of the trimeric assembly in Fig. 2a on the lipid bilayer region of the bicelle based on the data in **a–d**. The regions involved in TRAIL binding are shown in yellow.

**Table 1.** Binding properties of anti-DR5 NANOBODY® compounds.

NANOBODY® compound ID	Affinity by SPR ( $10^{-9}$ M)	DR5 selectivity	TRAIL blockade
NB1	6.7	Yes	No
NB2	1.0	Yes	No
NB3	7.3	Yes	Yes
NB4	4.2	Yes	Yes
NB5	0.17	Yes	Partial

between disruption of preligand cluster and receptor activation for DR5 (Fig. 5e). Since sdAbs are monovalent, achieving high levels of activity solely by interference with preligand association was rather unexpected, further highlighting the important role of preligand association in receptor autoinhibition. We also tested whether linking the synergistic sdAbs can further increase the agonistic property and found that covalently linking NB1 and NB3 (NB1–NB3) resulted in an  $EC_{50}$  of DR5 activation of  $\sim 0.78$  nM, which is  $\sim 13$  times lower than that of non-linked NB1 and NB3 combination and  $\sim 4$  times lower than that of TRAIL (Supplementary information, Fig. S6).

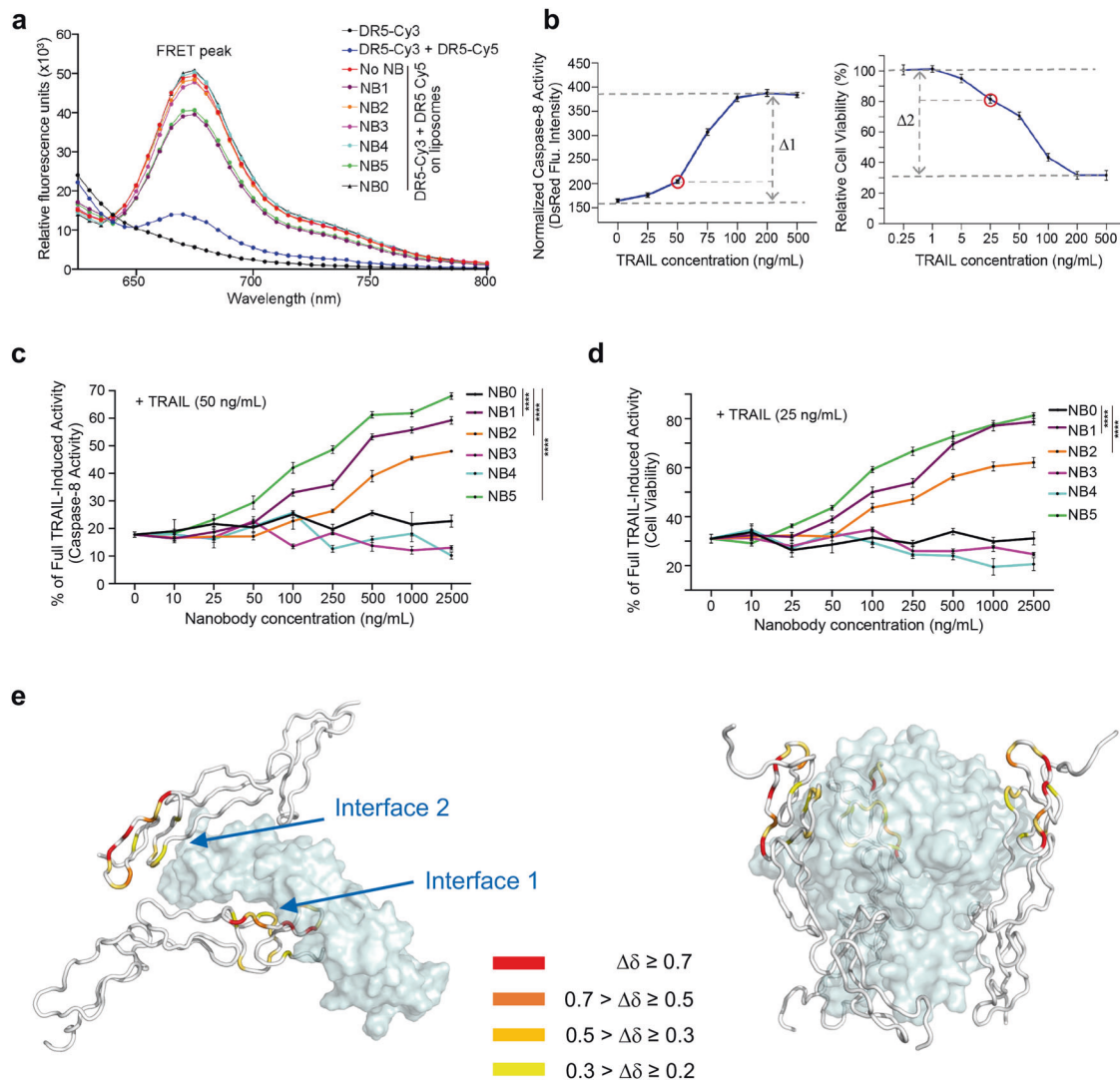


**Fig. 4** Interference with preligand association by sdAbs and influence on TRAIL-induced DR5 signaling. **a** Effect of the five NANOBODY® compounds (NB1–NB5) with high affinity for DR5-ECD (Table 1) on preligand association as reported by the liposome-based FRET assay. NB0 is a negative control sdAb that does not bind DR5-ECD. **b** TRAIL dose-response activation profiles based on caspase-8 activity (left) and cell viability (right). Monoclonal HEK293T stable cells expressing wild-type (WT) DR5 were treated with indicated concentrations of TRAIL for 6 h and 12 h for caspase-8 activity and cell viability readout, respectively. Caspase-8 activity was measured using the CaspGLOW red caspase-8 activity kit. Cell viability was measured using the cell-count kit (CCK-8) that measures dehydrogenase activity of the cells. Results were obtained from 3 independent experiments ( $n = 3$ ) and expressed as means  $\pm$  SEM. **c** Effect of sdAbs on DR5 signaling in the presence of 50 ng/mL TRAIL reported by caspase-8 activity as in **b**. HEK293T stable cells expressing WT DR5 were treated with indicated concentrations of sdAbs and 50 ng/mL TRAIL for 6 h. The reported activity is normalized as % of the fully saturated DR5 activation by TRAIL, indicated by  $\Delta 1$  in **b**. Results were obtained from 3 independent experiments ( $n = 3$ ) and expressed as means  $\pm$  SEM. Two-way ANOVA, \*\*\*\* $P < 0.0001$ . **d** Effect of sdAbs in the presence of 25 ng/mL TRAIL reported by cell viability as in **b**. HEK293T stable cells expressing WT DR5 were treated with indicated concentrations of sdAbs and 25 ng/mL TRAIL for 12 h. The reported activity is normalized as % of the fully saturated DR5 activation by TRAIL, indicated by  $\Delta 2$  in **b**. Results were obtained from 3 independent experiments ( $n = 3$ ) and expressed as means  $\pm$  SEM. Two-way ANOVA, \*\*\*\* $P < 0.0001$ . **e** Epitope mapping for NB1 by NMR. Residue-specific normalized chemical shift changes ( $\Delta\delta$ ; see Supplementary information, Fig. S4b for definition) are mapped onto the DR5-ECD preligand structure (left) and TRAIL-bound structure (right) according to the color spectrum defined in the figure.

#### Presence of DR5 preligand clusters on cell surface

The preligand association structure of DR5-ECD was determined in the absence of the transmembrane and membrane-proximal regions and in the context of rather artificial membrane environment. To test whether the self-association of DR5 characterized by NMR is represented in a more native setting, we implemented the split green fluorescence protein (GFP) assay<sup>46</sup> for both visualization and quantification of receptor clustering on cell surface using a more native construct including the ECD, the stalk sequence, and the monomeric form of TMD. In our previous study on DR5, we found that the TMD alone can form

structurally defined higher-order clusters if not physically constrained by the ECD, i.e., artificially shedding the DR5-ECD from the cell surface could activate DR5 to the full capacity.<sup>37</sup> Thus, to eliminate possible confounding effects from TMD clustering, we introduced two mutations, G217Y and A222Y, that have been shown to disrupt TMD dimerization and trimerization, respectively.<sup>37</sup> The resulting monomeric form of TMD is designated TMD<sup>m</sup>. The complementary GFP fragments from the Split-Venus system, GFP<sup>N</sup> and GFP<sup>C</sup>, were separately fused to the C-terminus of ECD-TMD<sup>m</sup> for providing fluorescent readout of receptor self-association. A Flag tag was fused to the N-terminus of ECD-TMD<sup>m</sup>



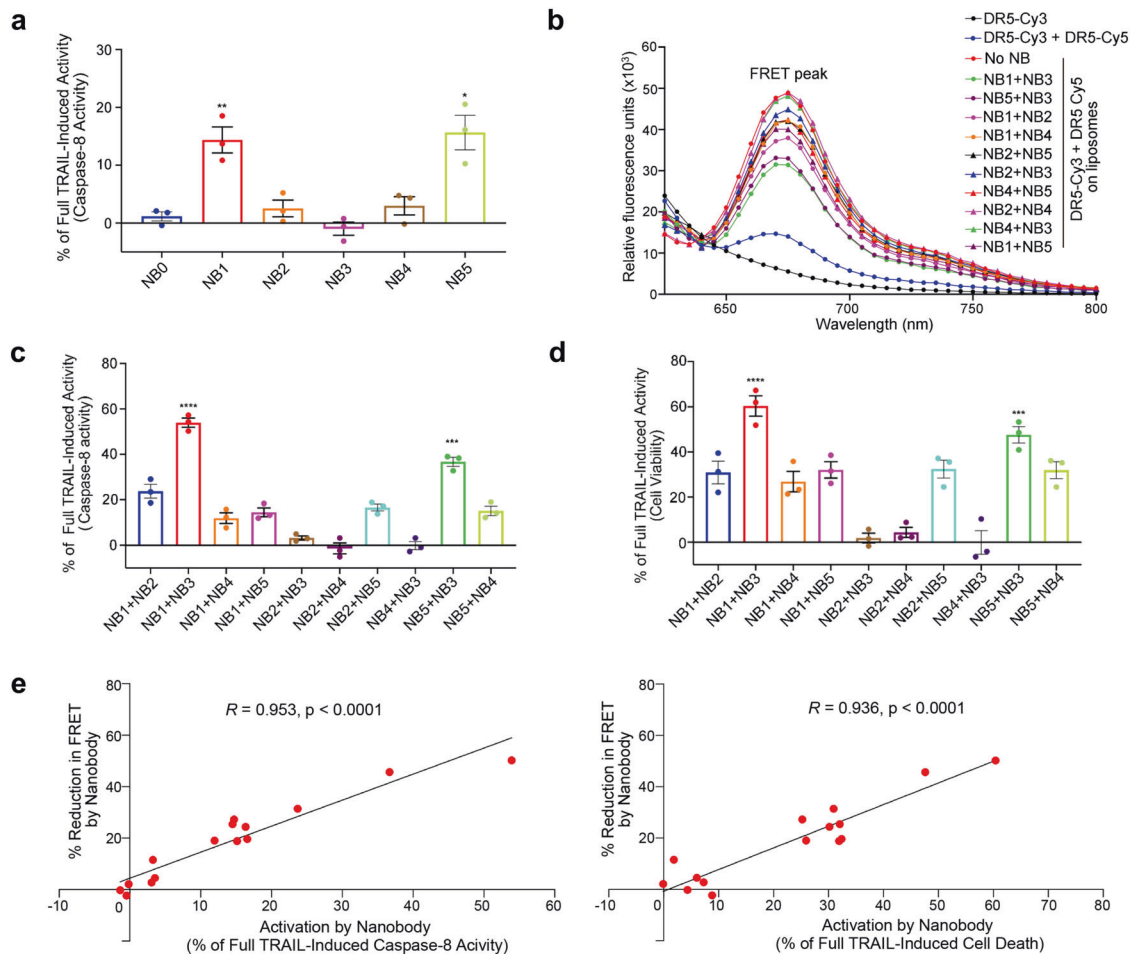


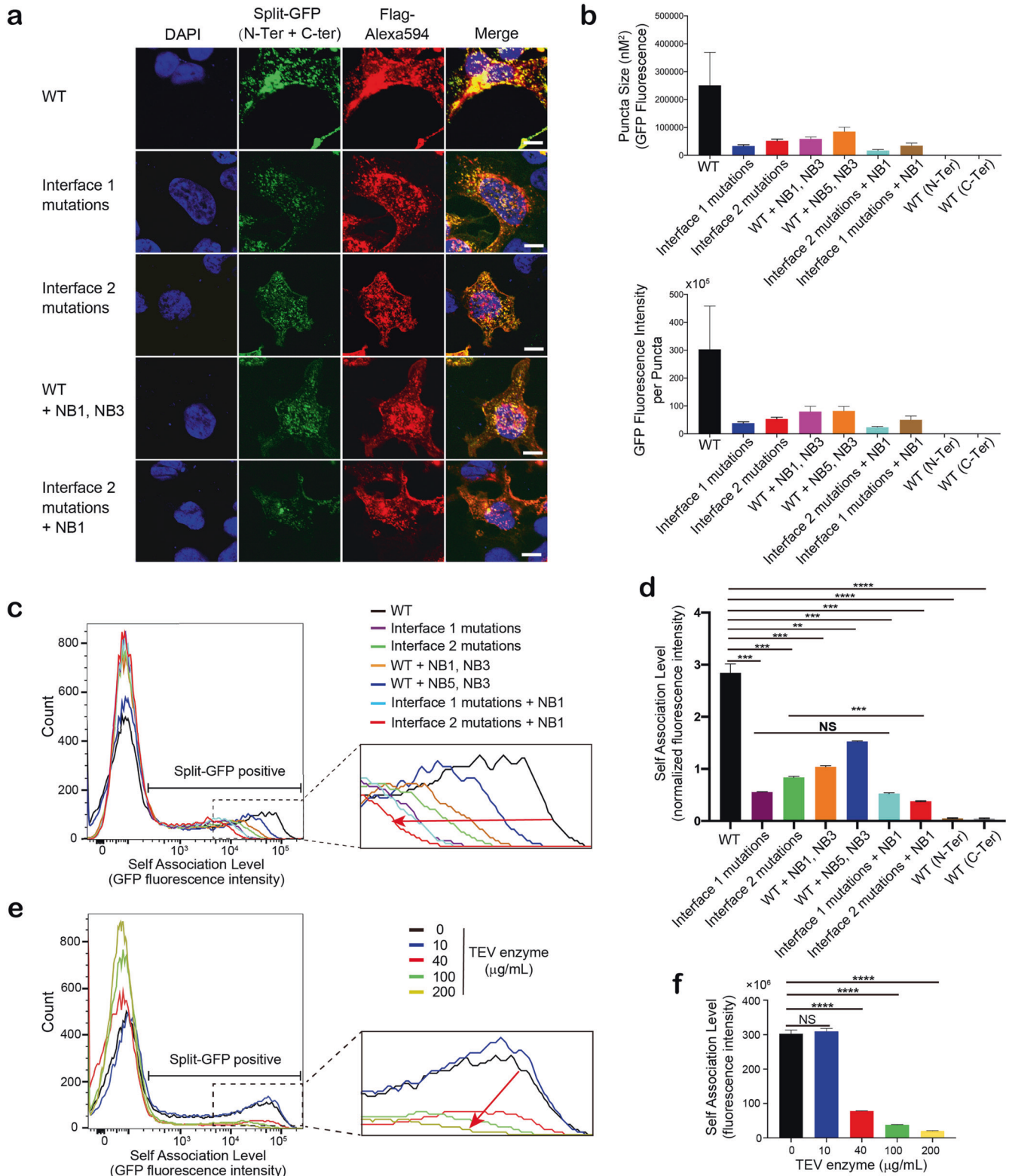
**Fig. 5 SdAb disruption of preligand association and agonistic effect in the absence of TRAIL.** **a** Effect of the five individual sdAbs on DR5 signaling as reported by caspase-8 activity in the absence of TRAIL (see also Supplementary information, Fig. S5a, b). Monoclonal HEK293T stable cells expressing WT DR5 were treated with 1  $\mu\text{g}/\text{mL}$  sdAbs for 6 h. Caspase-8 activity was measured using the CaspGLOW red caspase-8 activity kit and normalized as % of the fully saturated DR5 activation by TRAIL, indicated by  $\Delta 1$  in Fig. 4b. Results were obtained from 3 independent experiments ( $n = 3$ ) and expressed as means  $\pm$  SEM. Student's  $t$ -tests,  $*P < 0.05$ ,  $**P < 0.01$ . **b** Disruption of preligand association by all combinations of two sdAbs out of the five, as reported by the liposome-based FRET assay. **c** Effect of all combinations of two sdAbs in **b** on DR5 signaling reported by caspase-8 activity. HEK293T stable cell lines expressing the WT DR5 were treated with combinations of sdAbs (1  $\mu\text{g}/\text{mL}$  each) for 6 h (see also dose response in Supplementary information, Fig. S5c). Caspase-8 activity was measured and reported as in **a**. Student's  $t$ -tests,  $***P < 0.001$ ,  $****P < 0.0001$ . **d** Same as in **c** using cell viability as readout. HEK293T stable cells expressing WT DR5 were treated with combinations of sdAbs (1  $\mu\text{g}/\text{mL}$  each) for 12 h. Cell viability was measured and reported as in Fig. 4d. Student's  $t$ -tests,  $***P < 0.001$ ,  $****P < 0.0001$ . **e** Correlation between disruption of preligand association reported by FRET reduction and DR5 activation reported by caspase-8 activity (left) or cell viability (right). The results from all individual and pairs of sdAbs were combined to generate the plots.

for quantifying protein expression on the cell surface. Altogether, this construct is designated Flag-ECD-TMD<sup>m</sup>-GFP<sup>N/C</sup>. Moreover, a cleavable version of the construct Flag-ECD-tev-TMD<sup>m</sup>-GFP<sup>N/C</sup> was used as the negative control. The ECD part of the construct was mutated to test hypotheses. All split-GFP constructs are shown in Supplementary information, Fig. S7.

Co-expression of Flag-ECD-TMD<sup>m</sup>-GFP<sup>N</sup> and Flag-ECD-TMD<sup>m</sup>-GFP<sup>C</sup> with WT ECD in HEK293T cells resulted in strong GFP fluorescence and dense puncta (Fig. 6a), consistent with our hypothesis that two distinct preligand association of DR5-ECD can mediate the formation of higher-order clustering on the cell membrane. The TMD mutations did not seem to influence the preclustering of DR5-ECD because the same split-GFP construct with WT TMD showed very similar puncta size and intensity (Supplementary information, Fig. S8). As a negative control, separate expression of Flag-ECD-TMD<sup>m</sup>-GFP<sup>N</sup> or Flag-ECD-TMD<sup>m</sup>-GFP<sup>C</sup> did not show any GFP signal (Supplementary information, Fig. S9a). We then introduced mutations based on the structure to

disrupt Interface 1 (H85A, I95A, K98N, R115D) or Interface 2 (D120K, K155S, R154E, V165A), and found that both mutants exhibited 4–5 folds weaker GFP fluorescence and smaller puncta with the former being slightly more disruptive (Fig. 6a, b). Addition of sdAb combinations (NB1, NB3) or (NB5, NB3) during co-expression of the WT Flag-ECD-TMD<sup>m</sup>-GFP<sup>N</sup> and Flag-ECD-TMD<sup>m</sup>-GFP<sup>C</sup> also resulted in 2–3 folds less GFP signals (Fig. 6a, b; Supplementary information, Fig. S9b). We also tested the effect of NB1 on Interface 1 or 2 breaking mutants and found that combining NB1 with Interface 2 disrupting mutant yielded the weakest GFP signal, 7–8 folds less than the WT (Fig. 6a, b; Supplementary information Fig. S9b). The above differences in GFP fluorescence are significant because protein expression levels in all the test cases are very similar, as reported by anti-Flag fluorescent antibody (Supplementary information, Fig. S9c). The above constructs and test cases were also analyzed by flow cytometry and the results are in strong agreement with the cell imaging data (Fig. 6c, d; Supplementary information, Fig. S9d).





Notably, in the flow cytometry analysis, the combination of NB1 and Interface 2 breaking mutant also showed the largest reduction of GFP fluorescence. The NB1 binding site of DR5-ECD overlaps with Interface 1 but not Interface 2. Thus, combination of NB1, which disrupts Interface 1, with mutations that disrupt Interface 2 is expected to be the most inhibitory to the formation of preligand clusters.

The cleavable constructs Flag-ECD-tev-TMD<sup>m</sup>-GFP<sup>N</sup> and Flag-ECD-tev-TMD<sup>m</sup>-GFP<sup>C</sup>, when co-expressed, also showed strong GFP fluorescence and dense puncta as the non-cleavable ones but the fluorescence and puncta sharply reduced in the presence of TEV enzyme in a dose-independent manner (Fig. 6e, f; Supplementary information, Fig. S10a, b). The results indicate that the clustering of the Flag-ECD-TMD<sup>m</sup>-GFP<sup>N/C</sup> constructs observed in our studies

**Fig. 6 Examination of DR5-ECD preligand association on cell surface.** **a** Confocal images of DR5 ECD-TMD<sup>m</sup> and variants expressed in HEK293T cells in the absence and presence of sdAbs (see also Supplementary information, Fig. S9a). The constructs tested include the Flag-ECD-TMD<sup>m</sup>-GFP<sup>N/C</sup> with WT ECD and that with mutations disrupting Interface 1 (H85A, I95A, K98N, R115D) or Interface 2 (D120K, K155S, R154E, V165A). The sdAbs NB1 (1 µg/mL) and/or NB3 (1 µg/mL) were added before transfection. Cells were fixed with 4% paraformaldehyde and were then stained with Alexa Fluor® 594 anti-Flag antibody for 2 h before imaging (405 nm, 488 nm and 559 nm lasers were used for DAPI, split-GFP, and Alexa549 channels, respectively). Images were taken with the Olympus Fluoview FV1000 confocal microscope. Scale bar, 5 µm. **b** Quantification of the size (top) and intensity (bottom) of the puncta (or clusters) using the Fiji software. **c** Flow cytometry plots in the GFP fluorescence dimension, reporting self-association of Flag-ECD-TMD<sup>m</sup>-GFP<sup>N/C</sup> and variants expressed in HEK293T cells (see also Supplementary information, Fig. S9d). **d** Normalized split-GFP fluorescence intensity by dividing the integrated signals of the association-positive region (GFP fluorescence) by that of expression-positive region (Flag-Alexa647 fluorescence) in Supplementary information, Fig. S9d. Student's *t*-tests, \*\*\**P* < 0.01, \*\*\*\**P* < 0.001, \*\*\*\*\**P* < 0.0001 and NS (non-significant) represents *P* > 0.05. **e** Flow-cytometry plots in the GFP fluorescence dimension of Flag-ECD-tev-TMD<sup>m</sup>-GFP<sup>N/C</sup> in HEK293T cells in the presence of TEV enzyme (0–200 µg/mL; for dose-dependent removal of the ECD), showing that ECD self-association is responsible for the GFP signals in **a–d** (see also Supplementary information, Fig. 10a, b). **f** Quantification of data in **e** showing integrated signals in the split-GFP positive region at various protease concentrations. Student's *t*-tests, \*\*\*\**P* < 0.0001, and NS (non-significant) represents *P* > 0.05.

were solely caused by the ECD and that the mutated TMD (TMD<sup>m</sup>) could not have contributed significantly to oligomerization. Collectively, our cell imaging and flow cytometry data suggest that the specific structures of DR5 preligand association characterized by NMR are also represented on the cell surface.

## DISCUSSION

The fact that proteolytic removal of DR5-ECD can result in full receptor activation in the absence of ligand<sup>37</sup> implies that the oligomeric structures formed by membrane anchored ECD serves an autoinhibitory function. Indeed, we observed strong correlation between disruptions of DR5 preligand association by NANOBODY® compounds and receptor signaling (Fig. 5e). Of note, the NANOBODY® compounds are monovalent and thus their agonism cannot be attributed to receptor clustering by multivalent binding, a mechanism by which most known therapeutic antibodies are based on.<sup>47</sup> The DR5 signaling induced by NB1 and NB5 were solely due to disruption or loosening of the ECD preligand association by these molecules. In addition to the compounds tested in this study, there have been earlier reports of modifications of DR5-ECD that could augment receptor activity. A recent study identified a patch of positively charged residues (PPCR) involved in receptor autoinhibition, as mutational substitution and antibody-mediated PPCR interference resulted in increased apoptotic cytotoxic function of DR5.<sup>9</sup> In our preligand structure, the PPCR corresponds to <sup>154</sup>RKCR<sup>157</sup> and is a part of Interface 2 in which its basic residues are in position to form salt bridges with D120 and E151 of another monomer (Fig. 2b). This explains how mutating the basic residues of <sup>154</sup>RKCR<sup>157</sup> to acidic residues or sequestering <sup>154</sup>RKCR<sup>157</sup> with the antibody Lexatumumab can enhance DR5 activity by disrupting the preligand cluster. In another study, comprehensive genome profiling of human cancer cell lines found that TRAIL-sensitive cancer cells show markedly higher *O*-glycosylation of the ECD where Ser/Thr of residues 74–77 and 130–144 are putative sites of modification.<sup>48</sup> In our preligand structure, *O*-glycosylation of these sites are expected to cause steric hindrance at Interface 1 (Fig. 2b).

The preligand association domains (PLADs) of TNFR1 and Fas have been assigned to CRD1 and in both cases the self-association of PLAD has been implicated in promoting signaling.<sup>19–21</sup> For DR5, CRD1 is also the dominant PLAD that mediates preligand clustering, involved in both Interfaces 1 and 2, though CRD2 and CRD3 also contribute to intermolecular interactions (Fig. 2). The PLAD interactions of DR5 are, however, inhibitory as interference with the interactions all led to enhanced receptor activity. The discrepancy can be explained in two ways. First, the TMD of TNFR1 can only trimerize,<sup>35</sup> which implies that TNFR1 requires self-association of the CRD1 to achieve higher-order cluster upon ligand binding. In contrast, DR5-TMD can form multimer of trimer by itself to drive higher-order receptor clustering if not constrained by the preligand ECD.<sup>37</sup> Hence, while

DR5 PLAD is important for assembling the autoinhibitory, preligand cluster, the major function of TNFR1 PLAD may be mediating postligand clustering.<sup>35,49</sup> Second, preligand association has the dual functionality of gathering the receptors in preparation for ligand engagement while exerting autoinhibition to prevent receptor activation in the absence of ligand.

The general perception of receptor signaling is that activation is accompanied by higher-order clustering. However, in the case of DR5, it appears that higher-order preligand clusters are entirely possible without initiating signaling. We argue that despite being higher-order clusters, the preligand cluster is fundamentally different from the postligand cluster. First, the NMR PPT data indicate that DR5-ECD lies flat on membrane with the TRAIL binding site in a rather inaccessible position (Fig. 3e). Although no experimental data is available on the orientation of the DR5–TRAIL complex anchored to lipid bilayer, the ECD must be in the standing position by virtue of being complexed with the trimeric TRAIL. The footprint and thus receptor density of the preligand (resting) and postligand (standing) structures are significantly different (Fig. 7). Second, if the ECD C-termini positions are representative of the positions of the TMDs, the preligand and postligand clusters would result in very different TMD arrangements (Fig. 7). Given that the intracellular death domain and its adaptor protein can also form specific higher-order oligomeric signaling complex,<sup>50,51</sup> we argue that the dynamic clustering network of TMD compatible with intracellular oligomerization is likely the key determinant of activation. Indeed, when the TMD was mutated to not oligomerize, DR5 could no longer be activated even by proteolytic removal of its ECD (Supplementary information, Fig. S10c). Hence, the consequence of ligand binding may be converting a non-productive cluster to a signaling productive cluster.

In conclusion, there are genuine needs for in-depth understanding of the mechanism by which receptors in the TNFRSF are activated, as many of them are targets for antibody-based immunotherapy.<sup>24,26,52–54</sup> We find that the structural information of the preligand, autoinhibitory association of DR5, which is a representative member of the death receptors in the TNFRSF, can provide important clues for understanding the puzzling laboratory and disease phenotypes associated with modifications of DR5-ECD. Receptor preligand association is a vastly under explored area at the structural level due to technical challenges of working with dynamic and uncontrolled protein oligomerization. While direct visualization of large preligand clusters remains to be achieved by techniques such as cryo-electron microscopy or tomography, our study demonstrates the effective use of NMR, FRET, and sdAb binding for providing structural information of the interaction modules responsible for preligand association on lipid bilayer. Finally, the fact that monovalent molecules can modulate DR5 activity by interfering with preligand association suggests a new opportunity for developing agonistic molecules by targeting receptor preligand clustering.

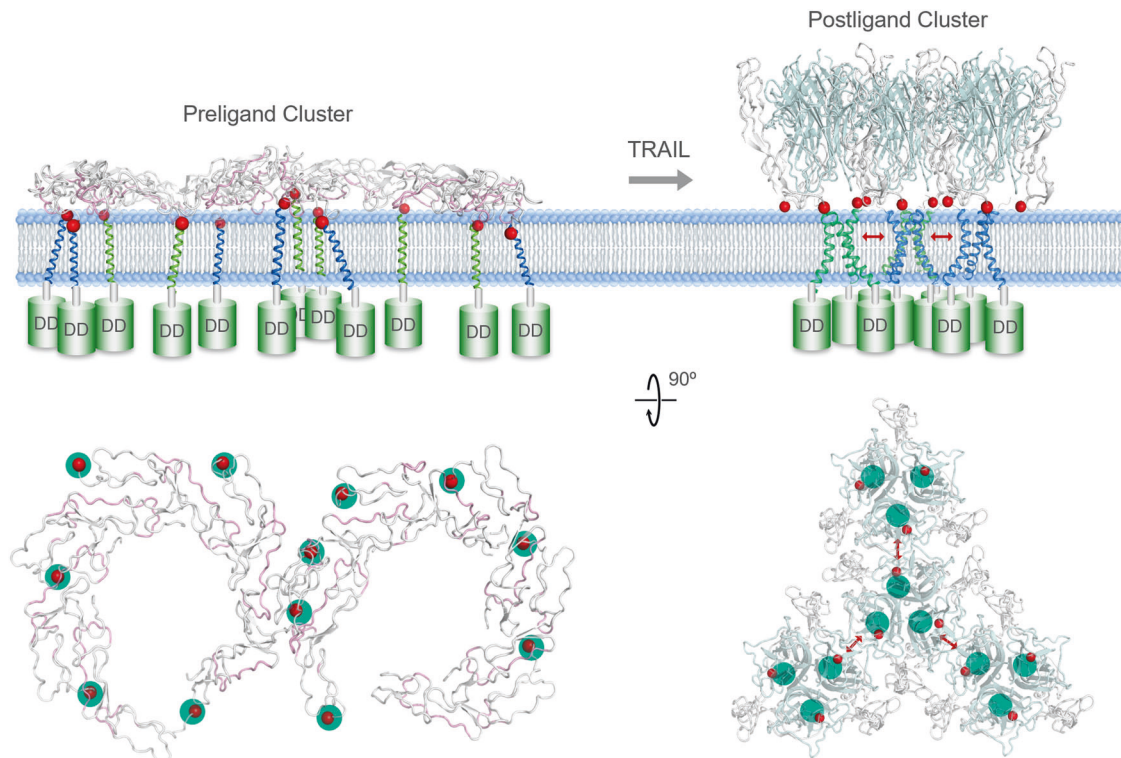


**Fig. 7 A model of receptor activation for DR5: converting preligand clusters (non-productive) to signaling-productive clusters.** The model posits that in the absence of ligand the ECD lies flat on membrane, forming clusters that position the TMDs in a loose arrangement incompatible with formation of the death-inducing signaling complex.<sup>69</sup> TRAIL binding causes the ECD to stand up, allowing the TMDs to cluster in a more compact dimer-trimer arrangement compatible with downstream signaling.<sup>37</sup> The red balls indicate the position of C-termini of the ECDs. The circles in cyan indicate the position of the TMDs. The pink regions in the resting state of ECDs indicate the TRAIL binding sites. “DD” denotes the intracellular death domain of DR5. The fundamentally different TMD patterns between the preligand and postligand states may be the key to explaining ligand-induced receptor activation.

## MATERIALS AND METHODS

### Protein expression and purification

DNA encoding the ectodomain of human DR5 (isoform 1), including residues 56–182 and designated DR5-ECD, was synthesized by GenScript (Piscataway, NJ). A 6× His-tag was appended to the C-terminus of DR5-ECD for purification and lipid bilayer anchoring. The DR5-ECD gene fragment was cloned into the pPICZα A vector for protein expression in yeast. Mutant DR5-ECD constructs were generated using the QuikChange II XL Site-Directed Mutagenesis Kit (Agilent Technologies, Cat# 200521) and confirmed by sequencing (Eton Bioscience Inc.). The expression plasmids were first amplified in *Escherichia coli* DH5α (New England Biolabs, Cat# C2987) cells, isolated using standard protocol, and linearized by the *SacI* enzyme. Then, 5–10 μg linearized DNA was transformed to *Pichia pastoris* yeast strain (X-33, Invitrogen, Cat# C18000) by electroporation. The transformed yeast cells were spread on separate YPD5 plates containing increasing concentration of Zeocin™ (100 μg/mL, 200 μg/mL, 500 μg/mL, 1000 μg/mL, 2000 μg/mL, InvivoGen, Cat# ant-zn-1p) to screen for high expressing clones. About 10 colonies were picked for small-scale expression test. The colony showing the highest expression level was subject to DNA sequencing as a final step of quality control. The X-33 cells were flash frozen in 15% glycerol and 85% YPD and stored at –80 °C for future protein expression.

For regular sample preparation, the X-33 cells were grown in Buffered Glycerol-complex Medium for 3 days at 30 °C. The cells were collected by centrifugation at 4000 rpm and resuspended in Buffered Methanol-complex Medium. Protein expression was induced by adding 0.5% v/v methanol every 24 h for 3 days. For NMR sample preparation, DR5-ECD expressing X-33 cells were grown in Buffered Minimal media with Glucose (BMGlc) with required isotopes. All isotopes used for protein isotope labeling were purchased from the Cambridge Isotope Laboratories. For <sup>15</sup>N labeling, 10 g <sup>15</sup>N ammonium sulfate was used per liter of BMGlc culture. For <sup>13</sup>C labeling, 5 g <sup>13</sup>C-glucose was used per liter of BMGlc culture. The cells were grown for 3 days at 30 °C and transferred to Buffered Minimal media with Methanol (BMMe) for induction as described previously.<sup>38,55</sup>

For <sup>15</sup>N labeling, 10 g <sup>15</sup>N ammonium sulfate was used per liter of BMMe culture. For <sup>13</sup>C labeling, one liter of BMGlc culture contained 0.5% v/v <sup>13</sup>C-methanol. Protein expression was induced by adding 0.5% methanol every 24 h for 3 days. For protein perdeuteration, cells were grown in BMGlc with 99.9% D<sub>2</sub>O and deuterated glucose, and protein expression was induced in BMMe with 99.9% D<sub>2</sub>O and deuterated methanol.

After induction, the cells were removed from the culture medium by centrifugation at 4000 rpm. The medium containing secreted DR5-ECD with C-terminal His-tag was passed through Ni-NTA resins (Sigma-Aldrich, Cat# 88223) in a gravity column (5 mL Ni-NTA resins per liter of culture medium). The Ni-NTA resins were washed first with 10× column volume of the HEPES Buffer A (20 mM HEPES and 150 mM NaCl, pH 7.5), then with 10× column volume of HEPES Buffer A with 20 mM imidazole (Sigma-Aldrich, Cat# I5513), and finally with 10× column volume of HEPES Buffer A with 30 mM imidazole. Protein was eluted in HEPES Buffer A with 300 mM imidazole, followed by dialysis against HEPES Buffer A to remove imidazole. In the final step, DR5-ECD was further purified by size-exclusion chromatography using a Superdex 200 Increase 10/300 GL (Cytiva) column in HEPES Buffer A (Supplementary information, Fig. S1a).

### Detection of preligand association by FRET

We first detected DR5-ECD self-association on liposomes by measuring FRET between Cy3- and Cy5- labeled DR5-ECDs when anchored to liposome. For this experiment, S77 in CRD1 was mutated to cysteine for fluorophore conjugation. Purified S77C mutant was dialyzed against 25 mM phosphate buffer (pH 6.0, degassed) and treated with 0.1 mM Tris(2-carboxyethyl) phosphine hydrochloride (TCEP, Sigma-Aldrich, Cat# C4706) for 20 min, followed by dialysis against 25 mM phosphate buffer (pH 6.0, degassed) for 4 h (buffer refreshed every hour) to remove TCEP completely. After dialysis, pH was adjusted to 7.5 and Cy3 (Sulfo-Cyanine3 maleimide, Lumiprobe, Cat# 21380) or Cy5 (Sulfo-Cyanine5 maleimide, Lumiprobe, Cat# 23380) in DMSO was immediately added to 10× protein concentration. The reaction sample was incubated at room temperature for 16 h in dark, followed by overnight



dialysis against the HEPES Buffer B (20 mM HEPES, 50 mM NaCl, pH 7.2) to remove free dye completely. To prepare liposomes for DR5-ECD anchoring, the 1,2-dioleoyl-sn-glycero-3-((N-(5-amino-1-carboxypentyl)iminodiacetic acid)succinyl) (nickel salt) (DGS-NTA (Ni), Avanti Polar Lipids, Cat# 790404 C), 1,2-Dimyristoyl-sn-Glycero-3-Phosphocholine (DMPC, Avanti Polar Lipids, Cat# 850345) were dissolved and mixed at the ratio of 1:10 in chloroform. The mixture was slowly dried to a thin film under nitrogen stream, followed by overnight lyophilization. The dried thin film was redissolved in HEPES Buffer B and then extruded through the 0.2  $\mu\text{m}$  Nuclepore™ Track-Etch membrane (Cytiva, Cat# 899-77053-P5) for 20 times by Mini-Extruder (Avanti Polar Lipids, Cat# 610020).

The Cy3-labeled and Cy5-labeled DR5-ECDs were first mixed at 1:1 ratio and then added to the liposomes. The final liposome sample contained 10  $\mu\text{M}$  DR5-ECD (5  $\mu\text{M}$  Cy3-labeled and 5  $\mu\text{M}$  Cy5-labeled), 127  $\mu\text{M}$  DGS-NTA (Ni), and 1272  $\mu\text{M}$  DMPC in HEPES Buffer B. Two hours after protein/liposome mixing to allow DR5-ECD oligomers to form, FRET was measured using SYNERGY microplate reader (Biotek) by excitation at 510 nm and recording of 520–800 nm spectrum (Fig. 1b).

### Preparation of DR5-ECD anchored to bicelles for NMR measurements

To prepare bicelles for DR5-ECD anchoring, DGS-NTA (Ni), DMPC (protonated or deuterated from Avanti Polar Lipids (Cat# 850345) or CortecNet (Cat# CD5011P025), respectively), and 1,2-diheptanoyl-sn-glycero-3-phosphocholine 7:0 PC (DH<sub>7</sub>PC; protonated or deuterated from Avanti Polar Lipids (Cat# 850306) and CortecNet (Cat# CD5011P025), respectively) were dissolved and mixed at a ratio of 1:10:22 in chloroform. The mixture was slowly dried to a thin film under nitrogen stream, followed by overnight lyophilization. The dried thin film was dissolved in HEPES Buffer B to form bicelles. The DR5-ECD sample to be anchored to the bicelles was dialyzed against HEPES Buffer B for 2 h, followed by concentration using Amicon Ultra Centrifugal Filter Units (3 kDa cut-off, Millipore, Cat# UFC900324). Concentrated protein sample was then gradually added to the bicelle solution to achieve desired protein and bicelle concentrations. The bicelle  $q$  was verified by 1D NMR as previously described.<sup>40</sup> Addition of DH<sub>7</sub>PC or reducing DH<sub>7</sub>PC by dialysis was used to adjust the bicelle  $q$  if needed. For most of the NMR measurements, the sample contained 400  $\mu\text{M}$  DR5-ECD, 4.4 mM DGS-NTA (Ni), 44 mM DMPC, 88 mM DH<sub>7</sub>PC, 20 mM HEPES and 50 mM NaCl (pH 7.2), and 5% D<sub>2</sub>O. At  $q = 0.5$ , the radius of the planar region of the bicelle is  $\sim 23 \text{ \AA}$ .<sup>56,57</sup> Assuming an area of  $\sim 60 \text{ \AA}^2$  per DMPC lipid,<sup>58</sup> there are  $\sim 55$  DMPCs per bicelle. Therefore, the molar ratio of protein to bicelle is  $\sim 1:2$ . For collecting NMR data for structural characterization, the freshly prepared NMR samples were left at room temperature for a day before NMR experiments at 37 °C.

### Analysis of time-dependent clustering of bicelle-anchored DR5-ECD by chemical crosslinking

DR5-ECD with C-terminal His-tag was expressed, purified, and reconstituted in DMPC-DH<sub>7</sub>PC bicelles ( $q = 0.5$ ) as described above. The sample was placed at 25 °C, and aliquot of 10  $\mu\text{L}$  was collected, immediately frozen in liquid nitrogen, and stored at  $-80^\circ\text{C}$  after 0, 1, 2, 3, 4 and 5 days. All collected aliquots from different time points were thawed and analyzed by chemical crosslinking at the same time. For chemical crosslinking, the aliquots were treated with 1 mM PEGylated bis(sulfosuccinimidyl)suberate (BS(PEG)9, Thermo Fisher Scientific, Cat# 21582) at pH 7.5 for 30 min, followed by incubation with 1 mM glutaraldehyde (Thermo Fisher Scientific, Cat# A17876.0F) for 5 min. The crosslinking reaction was quenched with a 20 mM Tris buffer (pH 7.5). The crosslinked species were examined by SDS-PAGE using the 4%–12% Bis-Tris protein gels (Thermo Fisher Scientific, Cat# NP0322BOX) at 200 V for 20 min, followed by Coomassie blue staining.

### Assignment of NMR resonances

All NMR data were collected at 30 °C or 37 °C on Bruker spectrometers operating at  $^1\text{H}$  frequency of 800 MHz, 700 MHz, or 600 MHz and equipped with cryogenic probes. NMR data were processed using NMRPipe<sup>59</sup> and spectra analysis was performed using XEASY<sup>60</sup> and CcpNmr Analysis v.2.<sup>61</sup> Sequence-specific assignment of backbone chemical shifts of free DR5-ECD was accomplished using three pairs of TROSY-enhanced triple resonance experiments,<sup>62,63</sup> including HNCA, HN(CO)CA, HN(CA)CO, HNCO, HNCACB, and HN(CO)CACB, recorded using a ( $^{15}\text{N}$ ,  $^{13}\text{C}$ , 85%  $^2\text{H}$ )-labeled sample at 30 °C and  $^1\text{H}$  frequency of 600 MHz. The N-terminal fragment (residues 56–76) was not assigned as most of the resonances were missing; this region is likely disordered. Out of 100 non-proline residues in residues

77–182, 95 were unambiguously assigned. The assignment of the bicelle-anchored DR5-ECD was achieved by tracing the free protein resonances while titrating the protein sample with DMPC-DH<sub>7</sub>PC bicelles with  $q = 0.5$ .

Having a relatively complete assignment of backbone  $^1\text{H}$  and  $^{15}\text{N}$  resonances, we recorded a 3D  $^1\text{H}^{\text{N}}\text{H}^{\text{N}}\text{N}$ -edited NOESY-TROSY spectrum ( $\tau_{\text{NOE}} = 200 \text{ ms}$ ) of a ( $^{15}\text{N}$ ,  $^2\text{H}$ )-labeled, bicelle-anchored sample at 37 °C and 800 MHz to assign  $\text{H}^{\text{N}}\text{H}^{\text{N}}$  NOEs. We found that essentially all  $\text{H}^{\text{N}}\text{H}^{\text{N}}$  NOEs (long and short range) are consistent with the crystal structure of DR5-ECD bound to TRAIL (PDB ID: 1D4V) (Supplementary information, Fig. S1c). Given that the structure of the bicelle-anchored DR5-ECD is essentially the same as the TRAIL-bound structure, assignment of sidechain resonances was achieved by analyzing regular NOESY spectra based on the crystal structure. We first assigned the aliphatic and aromatic resonances of free ( $^{15}\text{N}$ ,  $^{13}\text{C}$ )-labeled DR5-ECD using a combination of 3D  $^{15}\text{N}$ -edited NOESY-TROSY ( $\tau_{\text{NOE}} = 100 \text{ ms}$ ) and  $^{13}\text{C}$ -edited NOESY-HSQC ( $\tau_{\text{NOE}} = 150 \text{ ms}$ ) recorded at 37 °C and  $^1\text{H}$  frequency of 700 MHz. The assignment was based on consistency with the crystal structure. The assigned sidechain resonances were then traced using high resolution 2D  $^1\text{H}$ - $^{13}\text{C}$  HSQC recorded at 800 MHz when titrating the ( $^{15}\text{N}$ ,  $^{13}\text{C}$ )-labeled DR5-ECD with deuterated bicelles ( $q = 0.5$ ) to obtain sidechain assignments of bicelle-anchored DR5-ECD. The deuterated bicelle was prepared using DMPC and DH<sub>7</sub>PC with the acyl chains deuterated (CortecNet).

### Assignment of NOE restraints

Having the assignments of  $^1\text{H}$ - $^{13}\text{C}$  resonances of bicelle-anchored DR5-ECD, we assigned intramolecular NOEs using a combination of 3D  $^{15}\text{N}$ -edited NOESY-TROSY ( $\tau_{\text{NOE}} = 120 \text{ ms}$ ) and  $^{13}\text{C}$ -edited NOESY-HSQC ( $\tau_{\text{NOE}} = 150 \text{ ms}$ ) recorded at 37 °C and  $^1\text{H}$  frequency of 800 MHz using a sample of ( $^{15}\text{N}$ ,  $^{13}\text{C}$ )-labeled DR5-ECD anchored to deuterated bicelles ( $q = 0.5$ ). The intramolecular NOEs involving aliphatic protons are consistent with the crystal structure.

To detect intermolecular NOEs due to self-association of bicelle-anchored DR5-ECD, we first prepared an isotopically mixed sample containing 1:1 mixture of ( $^{15}\text{N}$ ,  $^2\text{H}$ )-labeled DR5-ECD and  $^{13}\text{C}$ -labeled DR5-ECD using an approach developed earlier for structure determination of transmembrane helix oligomers.<sup>40</sup> However, due to the large size of DR5-ECD oligomers on bicelles, filtering of intramolecular NOEs from residual aliphatic protons ( $<2\%$ ) using  $^1\text{H}$ - $^{13}\text{C}$  scalar coupling evolution caused too much signal loss and was thus not applicable. We therefore used a strategy that involves (1) splitting a ( $^{15}\text{N}$ ,  $^2\text{H}$ )-labeled sample to two halves, one mixed with  $^{13}\text{C}$ -labeled DR5-ECD at 1:1 ratio and the other not mixed, and (2) recording identical  $^{15}\text{N}$ -edited NOESY-TROSY spectra, which are highly sensitive, for the two samples. Specifically, the mixed sample contained 250  $\mu\text{M}$  ( $^{15}\text{N}$ ,  $^2\text{H}$ )-labeled and 250  $\mu\text{M}$   $^{13}\text{C}$ -labeled DR5-ECD in 1 mM bicelles (5.5 mM DGS-NTA, 55 mM DMPC and 110 mM DH<sub>7</sub>PC), and the negative-control sample contained 250  $\mu\text{M}$  ( $^{15}\text{N}$ ,  $^2\text{H}$ )-labeled DR5-ECD in the same bicelle solution. The  $^{15}\text{N}$ -edited NOESY-TROSY spectra were recorded with  $\tau_{\text{NOE}} = 200 \text{ ms}$  at 37 °C and  $^1\text{H}$  frequency of 800 MHz. Moreover, 2D  $^1\text{H}$ - $^{13}\text{C}$  HSQC spectrum of the mixed sample was recorded on the same spectrometer as an internal reference for the aliphatic proton chemical shifts. Intermolecular NOEs were assigned by direct comparison between the mixed and negative-control spectra (Supplementary information, Fig. S2a).

Analysis of intermolecular NOEs identified two non-overlapping regions of intermolecular contacts that cannot be accounted for by a single mode of protein–protein association, e.g., one interface is between CRD1 of one monomer and CRD2 of another monomer, and the other interface is between the opposite side of the CRD1 of one monomer and CRD3 of another monomer (Supplementary information, Fig. S2a). We therefore assigned two different interaction interfaces, which were further validated with intermolecular NOEs from a high-resolution 3D  $^{13}\text{C}$ -edited NOESY spectrum ( $\tau_{\text{NOE}} = 200 \text{ ms}$ ) recorded at 800 MHz (Supplementary information, Fig. S2b). In total, 61 intermolecular NOEs have been identified (37 for Interface 1 and 24 for Interface 2) (Supplementary information, Table S1).

### Structure calculation

Structure calculations were performed using the program XPLOR-NIH.<sup>64</sup> Structural characterization of DR5-ECD preligand association on bicelles involved two steps: (1) obtaining the structure of a monomeric subunit and (2) determining the oligomeric assembly that best satisfy the intermolecular NOE restraints. In the first step, we used the crystal structure as the starting model and refined it against NMR data collected for bicelle-anchored DR5-ECD, including all intramolecular NOE restraints and



backbone dihedral angles derived from  $^1\text{H}_\text{N}$ ,  $^{15}\text{N}$ ,  $^{13}\text{C}_\alpha$ ,  $^{13}\text{C}_\beta$ , and  $^{13}\text{C}'$  chemical shifts using the TALOS+ program.<sup>65</sup> For this step, we used a low-temperature simulated annealing (SA) protocol suitable for NMR based refinement of structural homology models<sup>66</sup> in which the temperature in the bath was cooled from 200 K to 20 K with steps of 20 K. The intramolecular NOE restraints were enforced by flat-well harmonic potentials, with the force constant ramped from 2 kcal/mol Å<sup>-2</sup> to 30 kcal/mol Å<sup>-2</sup> during annealing. Backbone dihedral angle restraints were taken from the “GOOD” dihedral angles from TALOS+, all with a flat-well ( $\pm$  the corresponding uncertainties from TALOS+) harmonic potential with force constant ramped from 30 kcal/mol rad<sup>-2</sup> to 300 kcal/mol rad<sup>-2</sup>. A total of 50 structures were calculated and the one with the lowest energy was selected for assembling the oligomer structures.

A minimum oligomeric number of three was required to cover the two distinct interaction interfaces defined by intermolecular NOEs and, hence, a trimer structure of DR5-ECD was computed to satisfy the NOE-derived distance restraints. We thus generated three identical copies of the monomer structure from Step 1 and employed the rigid-body dynamics feature during structure calculation of the oligomeric complex. Specifically, the backbone  $\text{C}_\alpha$  atoms of the structured regions of each monomer were grouped as a rigid-body to facilitate structure calculation while all sidechains were allowed to move. In this SA protocol, the temperature in the bath was cooled from 1000 K to 200 K with steps of 20 K. The NOE restraints (both inter- and intra-molecular) were enforced by flat-well harmonic potentials, with the force constant ramped from 2 kcal/mol Å<sup>-2</sup> to 30 kcal/mol Å<sup>-2</sup> during annealing. Backbone dihedral angle restraints were also applied, as in Step 1, with a flat-well harmonic potential with force constant ramped from 50 kcal/mol rad<sup>-2</sup> to 300 kcal/mol rad<sup>-2</sup>. A total of 100 structures were calculated and 15 lowest energy structures were selected as the final structural ensemble (Supplementary information, Fig. S2c and Table S1).

### Analysis of DR5-ECD orientation by paramagnetic probe titration

The resting position of DR5-ECD oligomeric complex on bicelles was examined by measuring PRE generated by two different lipophilic paramagnetic probes: N-TP (Avanti Polar Lipids, Cat# 810610P) and 5-DSA (Santa Cruz Biotech, Cat# sc-505955). For the N-TP probe, a single concentration of 2 mM was used with a bicelle sample consisting of 150  $\mu\text{M}$  DR5-ECD anchored to 300  $\mu\text{M}$  DMPC-DH<sub>7</sub>PC bicelle ( $q = 0.5$ ), which corresponds to  $\sim 6.7$  N-TP per bicelle. For PRE measurement, a purified sample of ( $^{15}\text{N}$ ,  $^2\text{H}$ )-labeled DR5-ECD was split into two halves, one mixed with bicelles and the other mixed with the same bicelle blended with N-TP. A 2D  $^1\text{H}$ - $^{15}\text{N}$  TROSY-HSQC spectrum was recorded for each of the samples at 700 MHz (with recovery delay of 3.5 s). PRE was defined as the ratio of peak intensity in the presence ( $I$ ) and absence ( $I_0$ ) of the paramagnetic agent.

For the 5-DSA probe, the PPT analysis<sup>40,43,67</sup> was performed using a sample comprising 400  $\mu\text{M}$  ( $^{15}\text{N}$ ,  $^2\text{H}$ )-labeled DR5-ECD and 800  $\mu\text{M}$  DMPC-DH<sub>7</sub>PC bicelles ( $q = 0.5$ ), which corresponds to 4.4 mM DGS-NTA (Ni), 44 mM DMPC, and 88 mM DH<sub>7</sub>PC. The sample was titrated with 5-DSA (40 mM stock solution in bicelles) to reach final 5-DSA concentrations of 0.5 mM, 2.0 mM, 3.0 mM, 4.0 mM, 6.0 mM and 7.0 mM, respectively. At each 5-DSA concentration, a 2D  $^1\text{H}$ - $^{15}\text{N}$  TROSY-HSQC spectrum was recorded at 700 MHz (with recovery delay of 3.5 s) to measure residue-specific PRE, defined here as the ratio of peak intensity in the presence ( $I$ ) and absence ( $I_0$ ) of the paramagnetic agent. For each of the residues, we used *Origin* (OriginLab, Northampton, MA) to fit the PRE titration curve to exponential decay

$$\frac{I}{I_0} = 1 - \text{PRE}_{\text{amp}} \left( 1 - e^{-[5\text{-DSA}]/\tau} \right) \quad (1)$$

to derive the residue-specific PRE amplitude ( $\text{PRE}_{\text{amp}}$ ).

### Examine higher-order oligomerization by intermolecular PRE

Intermolecular PRE was measured for cross validation of the NOE-derived interaction interfaces while potentially probing for higher-order oligomerization. Four mixed samples were prepared by mixing ( $^{15}\text{N}$ ,  $^2\text{H}$ )-labeled DR5-ECD with each of the following unlabeled DR5-ECD constructs containing a specific Cys mutation: S77C, S127C, S149C, and S183C, respectively. The WT and mutant proteins were purified as described above. The mutants with a free Cys, however, were first labeled with (1-Oxyl-2,2,5,5-tetramethylpyrrolidine-3-methyl) methanethiosulfonate (MTSL, Santa Cruz Biotech, Cat# sc-208677)

before mixing with ( $^{15}\text{N}$ ,  $^2\text{H}$ )-labeled DR5-ECD. For this, a purified Cys mutant was dialyzed against a 25 mM phosphate buffer (pH 6.0, degassed) and treated with 0.1 mM TCEP for 20 min, followed by dialysis against the same 25 mM phosphate buffer (pH 6.0, degassed) for 4 h (refresh buffer every hour) to remove TCEP completely. After dialysis, the pH was adjusted to 7.5 and MTSL (in DMSO) was immediately added to 10 $\times$  protein concentration. The reaction sample was incubated at room temperature for 16 h in dark, followed by overnight dialysis against HEPES Buffer B to remove free MTSL completely.

Each of the four MTSL-labeled mutants (NMR invisible) was mixed, at  $\sim 2:1$  molar ratio, with the ( $^{15}\text{N}$ ,  $^2\text{H}$ )-labeled DR5-ECD (for NMR readout). The mixed protein in solution was then anchored to DMPC-DH<sub>7</sub>PC bicelles with  $q = 0.5$ . Each of the four mixed samples comprised 100  $\mu\text{M}$  ( $^{15}\text{N}$ ,  $^2\text{H}$ )-labeled DR5-ECD, 200  $\mu\text{M}$  MTSL-mutant, and 600  $\mu\text{M}$  bicelles. In parallel, the reference sample comprising 100  $\mu\text{M}$  ( $^{15}\text{N}$ ,  $^2\text{H}$ )-labeled DR5-ECD, 200  $\mu\text{M}$  unlabeled WT DR5-ECD, and 600  $\mu\text{M}$  bicelles was prepared. Identical  $^1\text{H}$ - $^{15}\text{N}$  TROSY-HSQC spectra were recorded at 37  $^\circ\text{C}$  and 700 MHz for both samples for calculating PRE, defined as the ratio of peak intensity of the mixed spin-labeled sample ( $I$ ) to that of the mixed reference sample ( $I_0$ ). Note: we could not use 10–20 mM sodium ascorbate to reduce the MTSL to determine the reference peak intensity as this amount of ascorbate also reduced some of the seven native disulfide bonds.

### TRAIL preparation

Preparation of TRAIL used a protocol similar to that described previously.<sup>68</sup> DNA encoding residues 114–281 of human TRAIL was synthesized and subcloned into the pET28a(+) vector. The plasmid was transformed into *E. coli* strain BL21 (DE3) cells and grown in LB medium supplemented with 50  $\mu\text{g}/\text{mL}$  kanamycin (Sigma-Aldrich, Cat# BP861) at 37  $^\circ\text{C}$ . The incubator was cooled to 28  $^\circ\text{C}$  after the culture O.D. (600 nm) reached  $\sim 0.6$ , followed by induction with 100  $\mu\text{M}$  isopropyl  $\beta$ -D-thiogalactopyranoside (IPTG, Sigma-Aldrich, Cat# I5502) at 28  $^\circ\text{C}$  for 16 h. The cells were lysed by sonication in Lysis Buffer (100 mM  $\text{NaH}_2\text{PO}_4$ , 350 mM NaCl, pH 7.4). Soluble lysate was collected and loaded to Ni-NTA resin. After washing with Lysis Buffer supplemented with 20 mM imidazole, protein was eluted in the Lysis Buffer with 400 mM ammonium sulfate and 300 mM imidazole. Eluted protein was further purified by SEC using the Superdex 200 Increase 10/300 GL (Cytiva, Cat# GE28-9909-44) column in FPLC Buffer (100 mM  $\text{NaH}_2\text{PO}_4$ , 350 mM NaCl, 0.4 M  $(\text{NH}_4)_2\text{SO}_4$ , pH 7.4). The elution fractions containing pure TRAIL were collected, pooled and exchanged into the PBS buffer (pH 7.4) using PD10 column (GE, Healthcare, Cat# 17085101), followed by elimination of endotoxin using Pierce<sup>TM</sup> High Capacity Endotoxin Removal Spin Column (Thermo Fisher Scientific, Cat# 88274). Purified TRAIL solution was concentrated using Amicon Ultra Centrifugal Filter Units (10 kDa cut-off, Millipore, Cat# UFC901024), filtered (0.22  $\mu\text{m}$ ) and stored at  $-80^\circ\text{C}$  before use.

### NANOBODY<sup>®</sup> compound discovery and preparation

NANOBODY<sup>®</sup> compounds specific for DR5 have been previously described in a patent,<sup>45</sup> briefly to obtain these compounds, phage VHH libraries were synthesized from peripheral blood lymphocytes and lymph nodes from llamas immunized with soluble, recombinant fusion protein composed of human ectodomain of DR5 fused to hulgG1 Fc domain. Selection of hits was performed by up to two rounds of panning on human DR5 ectodomain fragments, and single clones were screened as *Escherichia coli* periplasmic extracts for binding to human and cynomolgus DR5 by ELISA. NANOBODY<sup>®</sup> candidates were selected based on their binding affinity to recombinant DR5 protein by surface plasmon resonance (SPR) using Biacore T100 and to DR5 expressed on COLO 205 cell line by flow cytometry. Additionally, the monomeric NANOBODY<sup>®</sup> compounds were subjected to thermal shift assay as a measure of inherent stability. The NANOBODY<sup>®</sup> candidates were also converted to multivalent formats via molecular cloning of repetitive glycine-serine polypeptide linkers between the building blocks. These multivalent formats were then evaluated for binding kinetics by SPR, induction of cell death and specificity of binding to DR5 by ELISA and protein chip analysis.

### Cell assay for sdAb- and ligand-induced DR5 activation

Human kidney epithelial cell line HEK293T and related DR5-expressing stable cell lines were maintained in DMEM (Thermo Fisher Scientific) plus 10% fetal bovine serum (Thermo Fisher Scientific), and 100 U/mL Pen-Strep (Thermo Fisher Scientific), at 37  $^\circ\text{C}$ , 5%  $\text{CO}_2$ .

**Stable cells.** Full-length human DR5 cDNA encoding isoform 1 (NCBI Ref. NP\_003833.4) was cloned into the pVCR8400-Puro vector (gift from the Springer Lab) to generate the plasmid for expressing the WT DR5. These plasmids were used with the HEK293T (ATCC, Cat# CRL-3216) cells to establish DR5-expressing stable cell lines. Briefly, 48 h after transfection, cells were treated with 2 mg/mL puromycin (Sigma-Aldrich, Cat# P8833). Clonal populations were produced by limited dilution, and individual clones were grown and checked for DR5 surface expression by using FITC-labeled anti-DR5 antibody (Abcam, Cat# ab53319). In vitro efficacy study was performed on the monoclonal stable HEK293T cells.

**Caspase-8 activity assay.** Cells were seeded at  $5 \times 10^4$  per well in 24-well plates. After 24 h, adherent cells were incubated with serial indicated concentrations of TRAIL (DR5 ligand), single sdAbs, combinations of sdAbs, linked NB1–NB3 (using 6× GGGGS linker) or sdAbs and TRAIL (50 ng/μL) for 6 h. After removing medium and adding 300 μL fresh medium, the Red-IETD-FMK (CaspGLOW red Caspase-8 activity kit, Biovision, Cat# K198) agent was added, and the plate was incubated at 37 °C for 1 h in an incubator with 5% CO<sub>2</sub>. After washing, cells were resuspended in 100 μL Wash Buffer (provided in the Kit) and transferred to black 96-well microtiter plate. Spectramax M5 Microplate Reader (Molecular Devices) (Ex/Em = 540/570 nm) was used to measure caspase-8 activation. Caspase-8 inhibitor IETD-FMK was conjugated to sulfo-rhodamine (Red-IETD-FMK, or DsRed2) as the fluorescent in situ marker to label apoptotic cells. Red-IETD-FMK is cell permeable, nontoxic, and irreversibly binds to activated caspase-8 in apoptotic cells.

**Cell viability assay.** Cells were seeded at  $10^4$  per well in 96-well plates. After 24 h, adherent cells were incubated with serial indicated concentrations of TRAIL (DR5 ligand), single sdAbs, combinations of sdAbs, linked NB1–NB3 (using 6× GGGGS linker), or sdAbs and TRAIL (25 ng/μL) for 12 h to allow full cytotoxic effect by ligand and/or sdAbs. Ultimately, cells were incubated with 10% (v/v) Cell count kit-8 (CCK-8, Dojindo, Cat# CK04) agent for 2 h. Absorbance at 450 nm was measured by using the spectramax M5 Microplate Reader (Molecular Devices).

## SEC-MALS analyses of DR5-ECD in complex with sdAbs or TRAIL

SEC-MALS experiments were performed using the Agilent 1260 Infinity Isocratic Liquid Chromatography System and SEPAX SRT SEC-300 column (Sepax Technologies; MW resolution range of 5–1250 kDa) with UV, LS, and RI detectors connected in series. For preparation of DR5-ECD in complex with sdAbs, DR5-ECD was mixed with NB1 or NB3 at molar ratio of 1:1 or mixed with NB1 and NB3 at molar ratio of 1:1:1, followed by purification by SEC (Superdex 200 Increase 10/300 GL column (Cytiva)). The purified samples of the complexes were then used for SEC-MALS analysis. For preparation of DR5-ECD in complex with sdAb and TRAIL, DR5-ECD, TRAIL and NB1 were mixed at molar ratio of 1:1:1.2 (TRAIL concentration calculated as monomer). The ternary complex was purified by SEC using the Superdex 200 Increase 10/300 GL column (Cytiva) column, followed by SEC-MALS analysis.

## Cell imaging

To examine whether the preligand association of DR5-ECD characterized by NMR exists on the cell membrane, we designed DR5 constructs in which the intracellular region (residues 245–440) was replaced by the N-terminal Venus fragment (strands 1–7; split-GFP N-Ter) or the C-terminal Venus fragment (strands 8–11; split-GFP C-Ter) for generating green fluorescence when the protein self-associate. Moreover, a Flag tag was added to the N-terminus of the ECD for quantifying protein expression on the cell surface. The construct is designated Flag-ECD-TMD<sup>m</sup>-GFP<sup>N/C</sup>.

The DNA encoding the Flag sequence (DYKDDDDK), human DR5 (isoform 1) residues 1–245 (ECD and TMD), and the N- or C-terminal Venus fragment was cloned into the pcDNA 3.1 vector (GenScript). The Interface 1 breaking mutant contained mutations H85A, I95A, K98N, and R115D. The Interface 2 breaking mutant contained mutations D120K, K155S, R154E, and V165A. To preclude the influence of TMD oligomerization that would reconstitute split-GFP fluorescence, two mutations, G217Y and A222Y, were introduced to the TMD. All mutations were introduced using the QuikChange II XL Site-Directed Mutagenesis Kit (Agilent Technologies, Cat# 200521). For proteolytic removal of the ECD by TEV enzyme, the TEV cleavage sequence (ENLYFQGGGGG) was inserted between the ECD and TMD after residue 208.

HEK293T cells were plated in 24-well plates at  $5 \times 10^4$  cells per well. After 24 h, WT or mutant Flag-ECD-TMD<sup>m</sup>-GFP<sup>N</sup> (50 ng) and Flag-ECD-TMD<sup>m</sup>-GFP<sup>C</sup> (48.3 ng) constructs were co-transfected at 1:1 molar ratio into HEK293T cells by using Lipofectamine 3000 (Invitrogen, Cat# L3000008). 18 h post transfection, cells were fixed by addition of 500 μL 4% paraformaldehyde in PBS at 37 °C for 15 min. After washing the coverslips twice with PBS, cells were blocked with 2% BSA in PBS for 30 min at room temperature. Cells were then incubated with Alexa Fluor® 594 anti-Flag antibody (Clone: L5) (BIOLEGEND Inc., Cat# 637314), diluted 200× in PBS buffer containing 2% BSA, at room temperature in the dark for 2 h. Following 3 washes with PBS, coverslips were mounted with ProLong Gold Antifade Mountant with DAPI (Thermo Fisher Scientific, Cat# P36941) onto slides and left to dry 1.5 h in the dark. Afterwards, all the images were taken using the Olympus Fluoview FV1000 confocal microscope.

For test cases involving the sdAbs, 1.0 μg/mL sdAb was added to the cell immediately after protein transfection to interfere with protein self-association during expression. After 18 h of expression, cells were stained and imaged as described above. For test cases involving TEV enzyme (James Chou lab), the DNAs of the cleavable constructs Flag-ECD-tev-TMD<sup>m</sup>-GFP<sup>N</sup> (50 ng) and Flag-ECD-tev-TMD<sup>m</sup>-GFP<sup>C</sup> (48.3 ng) were co-transfected at 1:1 molar ratio into HEK293T cells which were plated onto coverslips in 24-well plates at  $5 \times 10^4$  cells per well. After co-transfection, cells were treated with 10 μg/mL, 40 μg/mL, 100 μg/mL, or 200 μg/mL TEV enzyme for 18 h at 37 °C, followed by staining and imaging as described above.

## Flow cytometry

Protein constructs were made exactly as described above for cell imaging. HEK293T cells were plated onto 6-well plate at  $0.5 \times 10^6$  cells per well. After 24 h, WT or mutant Flag-ECD-TMD<sup>m</sup>-GFP<sup>N</sup> (400 ng) and Flag-ECD-TMD<sup>m</sup>-GFP<sup>C</sup> (386.4 ng) constructs were co-transfected at 1:1 molar ratio into HEK293T cells by using Lipofectamine 3000 (Invitrogen). 18 h posttransfection, cells were washed 2 times with cold Flow Cytometry Buffer (PBS containing 10% FBS) and stained with Alexa Fluor® 647 anti-Flag antibody (Clone: L5) (Biolegend Inc, Cat# 637316) diluted 50× in the Flow Cytometry Buffer for 1.5 h at 4 °C in the dark. After staining, the cells were washed again with cold Flow Cytometry Buffer 2 times and analyzed by flow cytometry (BD LSR-II Analyser).

For test cases involving the sdAbs, 1.0 μg/mL sdAb was added to the cell immediately after protein transfection to interfere with protein self-association during expression. After 18 h of expression, cells were stained and analyzed by flow cytometry (BD LSR-II Analyser) as described above. For test cases involving TEV enzyme, the DNAs of the cleavable constructs Flag-ECD-tev-TMD<sup>m</sup>-GFP<sup>N</sup> (400 ng) and Flag-ECD-tev-TMD<sup>m</sup>-GFP<sup>N</sup> (384.6 ng) were co-transfected at 1:1 molar ratio into HEK293T cells which were plated onto 6-well plate at  $0.5 \times 10^6$  cells per well. After co-transfection, cells were treated with 10 μg/mL, 40 μg/mL, 100 μg/mL, or 200 μg/mL TEV enzyme for 18 h at 37 °C, followed by staining and analyzing through flow cytometry as described above. The 633 nm laser with 670/20 band pass (BP) emission filter was used for Alexa fluor 647. The 488 nm laser was used to excite the split-GFP and measured with a 550/10 BP filter.

## Vector and plasmid information

Name	Source	Catalog
pVRC8400-puro	Tim Springer lab	N/A
pVRC-DR5 WT, for stable cell line	This paper	N/A
pVRC-DR5-TEV WT	This paper	N/A
pVRC-DR5-TEV MT (G217Y and A222Y)	This paper	N/A
pEYFP-N1 vector	Clontech	Cat# 6006-1
pECFP-N1 vector	Clontech	Cat# 6900-1
pcDNA3-GFP-LIC vector	Scott Gradia	Addgene plasmid # 30127
pcDNA3-GFP-DR5 WT	This paper	N/A
pET28a(+)-TRAIL114-281	GenScript	N/A
pPICZα A	GenScript	N/A

Name	Source	Catalog
pPICZα A-DR5-ECD-WT	GenScript	N/A
pPICZα A-DR5-ECD S77C	GenScript	N/A
pPICZα A-DR5-ECD S127C	GenScript	N/A
pPICZα A-DR5-ECD S149C	GenScript	N/A
pPICZα A-DR5-ECD S174C	GenScript	N/A
pPICZα A-DR5-ECD S183C	GenScript	N/A
pcDNA3.1-Flag-ECD <sup>WT</sup> -TMD <sup>m</sup> -GFP(Venus) <sup>N</sup>	GenScript	N/A
pcDNA3.1-Flag-ECD <sup>WT</sup> -TMD <sup>m</sup> -GFP(Venus) <sup>C</sup>	GenScript	N/A
pcDNA3.1-Flag-ECD <sup>WT</sup> -tev-TMD <sup>m</sup> -GFP(Venus) <sup>N</sup>	GenScript	N/A
pcDNA3.1-Flag-ECD <sup>WT</sup> -tev-TMD <sup>m</sup> -GFP(Venus) <sup>C</sup>	GenScript	N/A
pcDNA3.1-Flag-ECD <sup>Interface 1</sup> MT <sub>2</sub> -TMD <sup>m</sup> -GFP(Venus) <sup>N</sup>	This paper	N/A
pcDNA3.1-Flag-ECD <sup>Interface 1</sup> MT <sub>2</sub> -TMD <sup>m</sup> -GFP(Venus) <sup>C</sup>	This paper	N/A
pcDNA3.1-Flag-ECD <sup>Interface 2</sup> MT <sub>2</sub> -TMD <sup>m</sup> -GFP(Venus) <sup>N</sup>	This paper	N/A
pcDNA3.1-Flag-ECD <sup>Interface 2</sup> MT <sub>2</sub> -TMD <sup>m</sup> -GFP(Venus) <sup>C</sup>	This paper	N/A

### Quantification and statistical analysis

Statistical significance was calculated by using GraphPad Prism 6.01 (unpaired Student's *t*-test, <https://www.graphpad.com/scientific-software/prism/>). The number of independent experiment of duplicates, the statistical significance, and the statistical test used to determine the significance are indicated in each figure or figure legend or method section where quantification is reported.

### DATA AVAILABILITY

All data are available in the main text or the supplementary materials. The atomic structure coordinate and structural constraints have been deposited in the Protein Data Bank (PDB) with accession number 8DPX. The chemical shift values have been deposited in the Biological Magnetic Resonance Data Bank (BMRB) with accession number 31034.

### REFERENCES

- Chen, Z., Oh, D., Biswas, K. H., Zaidel-Bar, R. & Groves, J. T. Probing the effect of clustering on EphA2 receptor signaling efficiency by subcellular control of ligand-receptor mobility. *Elife* **10**, e67379 (2021).
- Janes, P. W., Nievergall, E. & Lackmann, M. Concepts and consequences of Eph receptor clustering. *Semin. Cell Dev. Biol.* **23**, 43–50 (2012).
- Zhang, X., Gureasko, J., Shen, K., Cole, P. A. & Kuriyan, J. An allosteric mechanism for activation of the kinase domain of epidermal growth factor receptor. *Cell* **125**, 1137–1149 (2006).
- Wu, H. Higher-order assemblies in a new paradigm of signal transduction. *Cell* **153**, 287–292 (2013).
- Dustin, M. L. & Groves, J. T. Receptor signaling clusters in the immune synapse. *Annu. Rev. Biophys.* **41**, 543–556 (2012).
- Graves, J. D. et al. Apo2L/TRAIL and the death receptor 5 agonist antibody AMG 655 cooperate to promote receptor clustering and antitumor activity. *Cancer Cell* **26**, 177–189 (2014).
- Hymowitz, S. G. et al. Triggering cell death: the crystal structure of Apo2L/TRAIL in a complex with death receptor 5. *Mol. Cell* **4**, 563–571 (1999).
- Adams, C. et al. Structural and functional analysis of the interaction between the agonistic monoclonal antibody Apomab and the proapoptotic receptor DR5. *Cell Death Diff.* **15**, 751–761 (2008).

- Shivange, G. et al. A patch of positively charged residues regulates the efficacy of clinical DR5 antibodies in solid tumors. *Cell Rep.* **37**, 109953 (2021).
- Schlessinger, J. Ligand-induced, receptor-mediated dimerization and activation of EGF receptor. *Cell* **110**, 669–672 (2002).
- Burgess, A. W. et al. An open-and-shut case? Recent insights into the activation of EGF/ErbB receptors. *Mol. Cell* **12**, 541–552 (2003).
- Reshetnyak, A. V. et al. Mechanism for the activation of the anaplastic lymphoma kinase receptor. *Nature* **600**, 153–157 (2021).
- Eck, M. J. & Sprang, S. R. The structure of tumor necrosis factor-α at 2.6 Å resolution. Implications for receptor binding. *J. Biol. Chem.* **264**, 17595–17605 (1989).
- Compaan, D. M. & Hymowitz, S. G. The crystal structure of the costimulatory OX40-OX40L complex. *Structure* **14**, 1321–1330 (2006).
- Banner, D. W. et al. Crystal structure of the soluble human 55 kd TNF receptor-human TNF beta complex: implications for TNF receptor activation. *Cell* **73**, 431–445 (1993).
- Mongkolsapaya, J. et al. Structure of the TRAIL-DR5 complex reveals mechanisms conferring specificity in apoptotic initiation. *Nat. Struct. Biol.* **6**, 1048–1053 (1999).
- Himanen, J. P. et al. Architecture of Eph receptor clusters. *Proc. Natl. Acad. Sci. USA* **107**, 10860–10865 (2010).
- Wang, F. et al. Structures of mouse and human GITR-GITRL complexes reveal unique TNF superfamily interactions. *Nat. Commun.* **12**, 1378 (2021).
- Chan, F. K. et al. A domain in TNF receptors that mediates ligand-independent receptor assembly and signaling. *Science* **288**, 2351–2354 (2000).
- Naismith, J. H., Devine, T. Q., Brandhuber, B. J. & Sprang, S. R. Crystallographic evidence for dimerization of unliganded tumor necrosis factor receptor. *J. Biol. Chem.* **270**, 13303–13307 (1995).
- Siegel, R. M. et al. Fas preassociation required for apoptosis signaling and dominant inhibition by pathogenic mutations. *Science* **288**, 2354–2357 (2000).
- Kumar, R. et al. Increased sensitivity of antigen-experienced T cells through the enrichment of oligomeric T cell receptor complexes. *Immunity* **35**, 375–387 (2011).
- Kramer, J. M. et al. Evidence for ligand-independent multimerization of the IL-17 receptor. *J. Immunol.* **176**, 711–715 (2006).
- Ashkenazi, A. Targeting the extrinsic apoptosis pathway in cancer. *Cytokine Growth Factor Rev.* **19**, 325–331 (2008).
- Watts, T. H. TNF/TNFR family members in costimulation of T cell responses. *Ann. Rev. Immunol.* **23**, 23–68 (2005).
- Wajant, H. Principles of antibody-mediated TNF receptor activation. *Cell Death Differ.* **22**, 1727–1741 (2015).
- Aggarwal, B. B. Signaling pathways of the TNF superfamily: a double-edged sword. *Nat. Rev. Immunol.* **3**, 745–756 (2003).
- Locksley, R. M., Killeen, N. & Lenardo, M. J. The TNF and TNF receptor super-families: integrating mammalian biology. *Cell* **104**, 487–501 (2001).
- Bodmer, J. L., Schneider, P. & Tschoop, J. The molecular architecture of the TNF superfamily. *Trends Biochem. Sci.* **27**, 19–26 (2002).
- Vanamee, E. S. & Faustman, D. L. Structural principles of tumor necrosis factor superfamily signaling. *Sci. Signal.* **11**, eaao4910 (2018).
- Karathanasis, C. et al. Single-molecule imaging reveals the oligomeric state of functional TNFα-induced plasma membrane TNFR1 clusters in cells. *Sci. Signal.* **13**, eaax5647 (2020).
- Fu, Q. et al. Structural basis and functional role of intramembrane trimerization of the Fas/CD95 death receptor. *Mol. Cell* **61**, 602–613 (2016).
- Valley, C. C. et al. Tumor necrosis factor-related apoptosis-inducing ligand (TRAIL) induces death receptor 5 networks that are highly organized. *J. Biol. Chem.* **287**, 21265–21278 (2012).
- Bitra, A. et al. Crystal structure of murine 4-1BB and its interaction with 4-1BBL support a role for galectin-9 in 4-1BB signaling. *J. Biol. Chem.* **293**, 1317–1329 (2018).
- Zhao, L., Fu, Q., Pan, L., Piai, A. & Chou, J. J. The diversity and similarity of transmembrane trimerization of TNF receptors. *Front. Cell Dev. Biol.* **8**, 569684 (2020).
- Goh, E. T. H. et al. A small molecule targeting the transmembrane domain of death receptor p75(NTR) induces melanoma cell death and reduces tumor growth. *Cell Chem. Biol.* **25**, 1485–1494.e5 (2018).
- Pan, L. et al. Higher-order clustering of the transmembrane anchor of DR5 drives signaling. *Cell* **176**, 1477–1489.e14 (2019).
- Pickford, A. R. & O'Leary, J. M. Isotopic labeling of recombinant proteins from the methylotrophic yeast *Pichia pastoris*. *Methods Mol. Biol.* **278**, 17–33 (2004).
- Li, B. et al. Activation of the proapoptotic death receptor DR5 by oligomeric peptide and antibody agonists. *J. Mol. Biol.* **361**, 522–536 (2006).
- Fu, Q., Piai, A., Chen, W., Xia, K. & Chou, J. J. Structure determination protocol for transmembrane domain oligomers. *Nat. Protoc.* **14**, 2483–2520 (2019).
- Battiste, J. L. & Wagner, G. Utilization of site-directed spin labeling and high-resolution heteronuclear nuclear magnetic resonance for global fold determination of large proteins with limited nuclear overhauser effect data. *Biochemistry* **39**, 5355–5365 (2000).



42. Clore, G. M. & Iwahara, J. Theory, practice, and applications of paramagnetic relaxation enhancement for the characterization of transient low-population states of biological macromolecules and their complexes. *Chem. Rev.* **109**, 4108–4139 (2009).
43. Piai, A., Fu, Q., Dev, J. & Chou, J. J. Optimal bicelle size  $q$  for solution NMR studies of the protein transmembrane partition. *Chemistry* **23**, 1361–1367 (2017).
44. Piai, A. et al. Structural basis of transmembrane coupling of the HIV-1 envelope glycoprotein. *Nat. Commun.* **11**, 2317 (2020).
45. Cromie, K. et al. Agonist DR5 binding polypeptides. WO2011/098520 A1 (2011).
46. Romei, M. G. & Boxer, S. G. Split green fluorescent proteins: scope, limitations, and outlook. *Annu. Rev. Biophys.* **48**, 19–44 (2019).
47. Huet, H. A. et al. Multivalent nanobodies targeting death receptor 5 elicit superior tumor cell killing through efficient caspase induction. *MAbs* **6**, 1560–1570 (2014).
48. Wagner, K. W. et al. Death-receptor O-glycosylation controls tumor-cell sensitivity to the proapoptotic ligand Apo2L/TRAIL. *Nat. Med.* **13**, 1070–1077 (2007).
49. Lo, C. H. et al. Noncompetitive inhibitors of TNFR1 probe conformational activation states. *Sci. Signal.* **12**, aav5637 (2019).
50. Wang, L. et al. The Fas-FADD death domain complex structure reveals the basis of DISC assembly and disease mutations. *Nat. Struct. Mol. Biol.* **17**, 1324–1329 (2010).
51. Scott, F. L. et al. The Fas-FADD death domain complex structure unravels signalling by receptor clustering. *Nature* **457**, 1019–1022 (2009).
52. Croft, M., Benedict, C. A. & Ware, C. F. Clinical targeting of the TNF and TNFR superfamilies. *Nat. Rev. Drug Discov.* **12**, 147–168 (2013).
53. Rogers, P. R., Song, J., Gramaglia, I., Killeen, N. & Croft, M. OX40 promotes Bcl-xL and Bcl-2 expression and is essential for long-term survival of CD4 T cells. *Immunity* **15**, 445–455 (2001).
54. Sheridan, J. P. et al. Control of TRAIL-induced apoptosis by a family of signaling and decoy receptors. *Science* **277**, 818–821 (1997).
55. Morgan, W. D., Kragt, A. & Feeney, J. Expression of deuterium-isotope-labelled protein in the yeast *Pichia pastoris* for NMR studies. *J. Biomol. NMR* **17**, 337–347 (2000).
56. Vold, R. R. & Prosser, R. S. Magnetically oriented phospholipid bilayered micelles for structural studies of polypeptides. Does the ideal bicelle exist? *J. Magn. Res. Ser. B* **113**, 267–271 (1996).
57. Sanders, C. R. 2nd & Schwonek, J. P. Characterization of magnetically orientable bilayers in mixtures of dihexanoylphosphatidylcholine and dimyristoylphosphatidylcholine by solid-state NMR. *Biochemistry* **31**, 8898–8905 (1992).
58. Kucerka, N. et al. Structure of fully hydrated fluid phase DMPC and DLPC lipid bilayers using X-ray scattering from oriented multilamellar arrays and from unilamellar vesicles. *Biophys. J.* **88**, 2626–2637 (2005).
59. Delaglio, F. et al. NMRPipe: a multidimensional spectral processing system based on UNIX pipes. *J. Biomol. NMR* **6**, 277–293 (1995).
60. Bartels, C., Xia, T. H., Billeter, M., Guntert, P. & Wuthrich, K. The program XEASY for computer-supported NMR spectral analysis of biological macromolecules. *J. Biomol. NMR* **6**, 1–10 (1995).
61. Vranken, W. F. et al. The CCPN data model for NMR spectroscopy: development of a software pipeline. *Proteins* **59**, 687–696 (2005).
62. Salzmann, M., Wider, G., Pervushin, K. & Wuthrich, K. Improved sensitivity and coherence selection for  $[15\text{N}, 1\text{H}]$ -TROSY elements in triple resonance experiments. *J. Biomol. NMR* **15**, 181–184 (1999).
63. Kay, L. E., Ikura, M., Tschudin, R. & Bax, A. Three-dimensional triple-resonance NMR spectroscopy of isotopically enriched proteins. *J. Magn. Reson.* **213**, 423–441 (1990).
64. Schwieters, C. D., Kuszewski, J., Tjandra, N. & Clore, G. M. The Xplor-NIH NMR molecular structure determination package. *J. Magn. Reson.* **160**, 66–74 (2002).
65. Shen, Y., Delaglio, F., Cornilescu, G. & Bax, A. TALOS+: a hybrid method for predicting protein backbone torsion angles from NMR chemical shifts. *J. Biomol. NMR* **44**, 213–223 (2009).
66. Chou, J. J., Li, S., Klee, C. B. & Bax, A. Solution structure of  $\text{Ca}^{2+}$ -calmodulin reveals flexible hand-like properties of its domains. *Nat. Struct. Biol.* **8**, 990–997 (2001).
67. Piai, A., Dev, J., Fu, Q. & Chou, J. J. Stability and water accessibility of the trimeric membrane anchors of the HIV-1 envelope spikes. *J. Am. Chem. Soc.* **139**, 18432–18435 (2017).
68. Ashkenazi, A. et al. Safety and antitumor activity of recombinant soluble Apo2 ligand. *J. Clin. Invest.* **104**, 155–162 (1999).
69. Kischkel, F. C. et al. Cytotoxicity-dependent APO-1 (Fas/CD95)-associated proteins form a death-inducing signaling complex (DISC) with the receptor. *EMBO J.* **14**, 5579–5588 (1995).

## ACKNOWLEDGEMENTS

This work was supported by NIH grants GM140887 (to J.J.C.) and AI150709 (to J.J.C. and H.W.). The NMR data were collected at the MIT-Harvard CMR (supported by NIH grants P41 GM132079 and S10 OD023513).

## AUTHOR CONTRIBUTIONS

G.D., L.Z., H.W., and J.J.C. conceived the study; G.D. and L.Z. prepared samples and performed NMR analyses; G.D. and J.J.C. determined the structures; Y.Z. and G.D. performed sAb analyses; A.B. and T.C. performed initial feasibility study of DR5 ECD; G.D. performed the FRET and cell assays; G.D., L.Z., and B.X. performed split-GFP experiments; K.H., K.V.D.H., M.-A.B., M.B., and L.-L.L. developed and prepared NANOBODY® compounds; J.J.C. and G.D. wrote the manuscript and all others helped with editing the manuscript.

## COMPETING INTERESTS

The authors declare no competing interests.

## ADDITIONAL INFORMATION

**Supplementary information** The online version contains supplementary material available at <https://doi.org/10.1038/s41422-022-00755-2>.

**Correspondence** and requests for materials should be addressed to Hao Wu or James Jiwei Chou.

**Reprints and permission information** is available at <http://www.nature.com/reprints>

Springer Nature or its licensor (e.g. a society or other partner) holds exclusive rights to this article under a publishing agreement with the author(s) or other rightsholder(s); author self-archiving of the accepted manuscript version of this article is solely governed by the terms of such publishing agreement and applicable law.



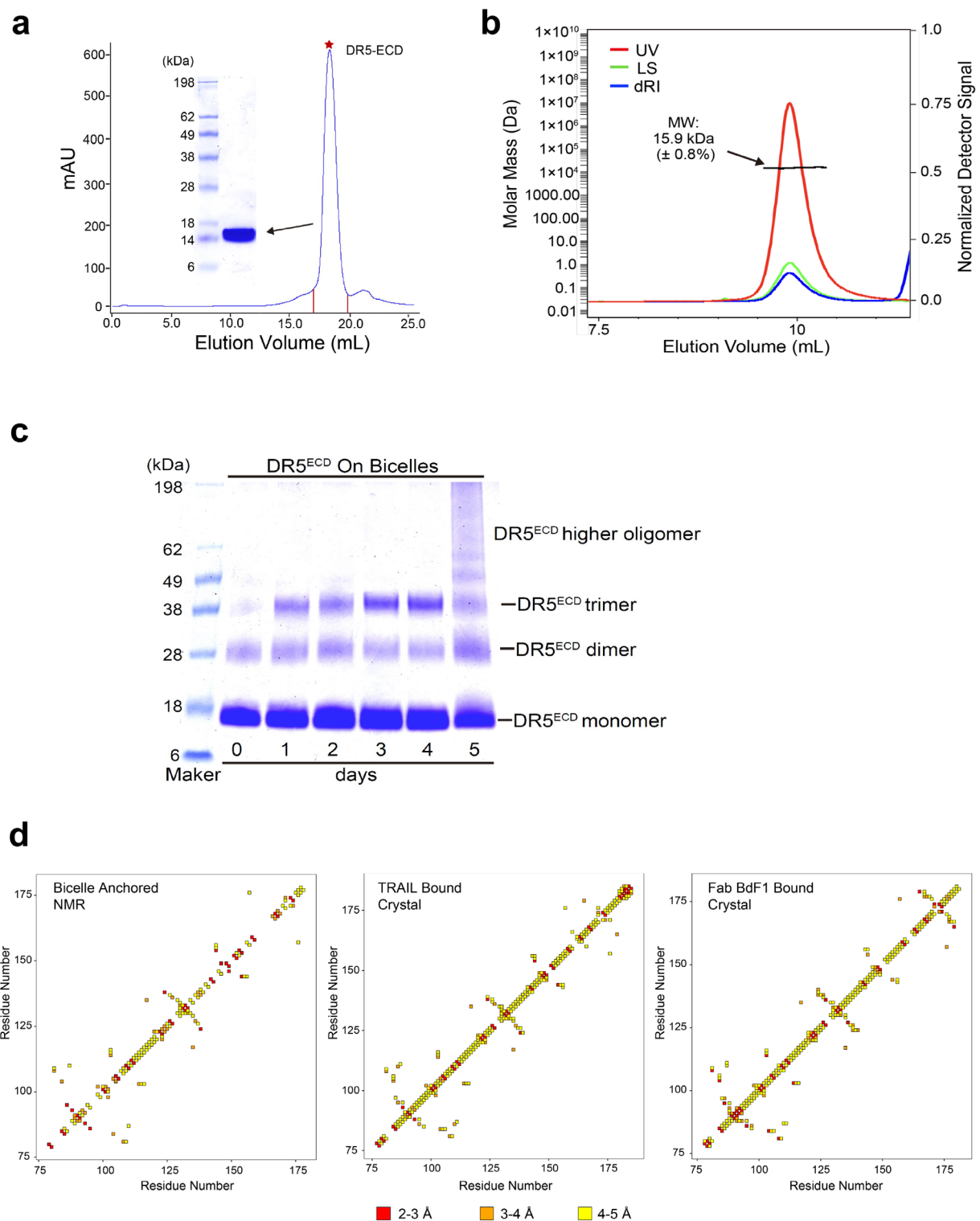


**Fig. S1: Additional biochemical and NMR characterization of DR5-ECD, related to Figs. 1 and 2**

**a** Typical size exclusion chromatogram of DR5-ECD on a Superdex 200 Increase 10/300 GL column and SDS-PAGE analysis for showing the purity of DR5-ECD used in this study.

**b** Size Exclusion Chromatography coupled to Multi Angle Light Scattering (SEC-MALS) analysis of DR5-ECD in solution. Chromatograms show the readings from the LS (green), RI (blue), and UV (red) detectors. The left and right axes represent the molecular mass and normalized detector signal, respectively. The black line represents the calculated molecular mass from MALS and UV/RI, and the average mass of the elution peak of DR5-ECD is 15.9 kDa, which corresponds to a monomer (theoretical MW of 15.5 kDa).

**c** Chemical crosslinking of DR5-ECD anchored to DMPC-DH<sub>7</sub>PC bicelles with  $q = 0.5$  after placed at room temperature for 0, 1, 2, 3, 4, and 5 days (lanes labeled accordingly). Details of crosslinking described in Materials and methods.

**d** Comparison of backbone H<sup>N</sup>-H<sup>N</sup> distances derived from H<sup>N</sup>-H<sup>N</sup> NOEs of bicelle-anchored DR5-ECD (left panel) with those derived from the crystal structures of DR5-ECD bound to TRAIL (middle panel) and antibody BdF1 (right panel). The H<sup>N</sup>-H<sup>N</sup> contact patterns are shown in a contact matrix representation. The PDB ID codes are: 1D4V for complex with TRAIL and 2H9G for complex with the Fab BdF1.

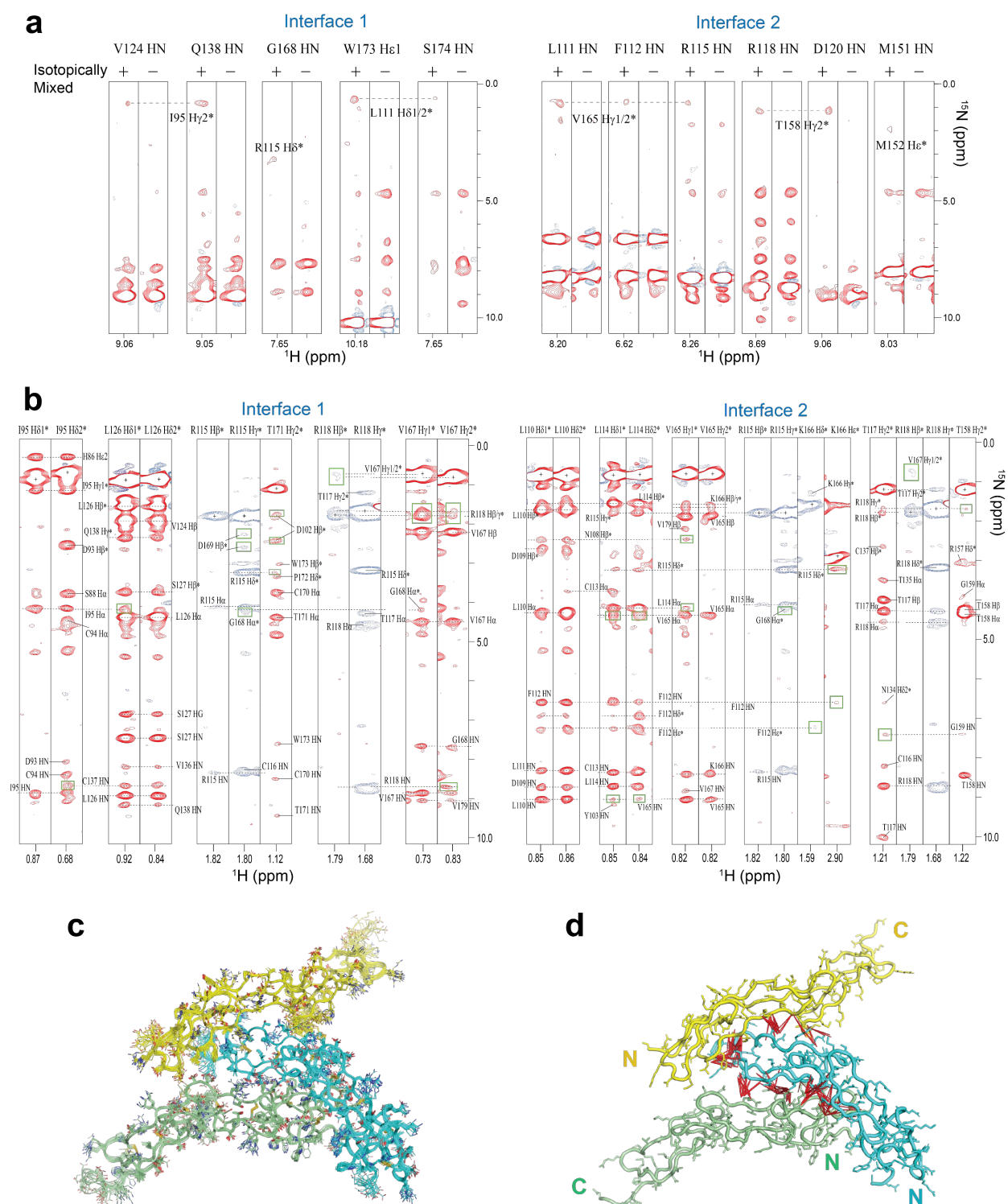


**Fig. S2: Structure determination of DR5-ECD preligand associations by NMR, related to Fig. 2**

**a** Sample NOE strips from 3D  $^{15}\text{N}$ -edited NOESY-TROSY-HSQC spectra recorded with  $\tau_{\text{NOE}} = 200$  ms using an isotopically mixed sample (left strips) and a control sample (right strips). The mixed sample consists of 0.25 mM ( $^{15}\text{N}$ ,  $^2\text{H}$ )-labeled DR5-ECD and 0.25 mM  $^{13}\text{C}$ -labeled DR5-ECD anchored to DMPC-DH<sub>7</sub>PC bicelles ( $q = 0.5$ ). The control sample contains 0.25 mM ( $^{15}\text{N}$ ,  $^2\text{H}$ )-labeled DR5-ECD prepared in the same way. Both samples contain 1 mM DMPC-DH<sub>7</sub>PC bicelles ( $q = 0.5$ ), which corresponds to 5.5 mM DGS-NTA (Ni), 55 mM DMPC, and 110 mM DH<sub>7</sub>PC. The spectra were recorded at 37°C and  $^1\text{H}$  frequency of 800MHz. The intermolecular NOE crosspeaks between amides and aliphatic protons due to the mixing of different isotopically labeled DR5-ECDs are labeled.

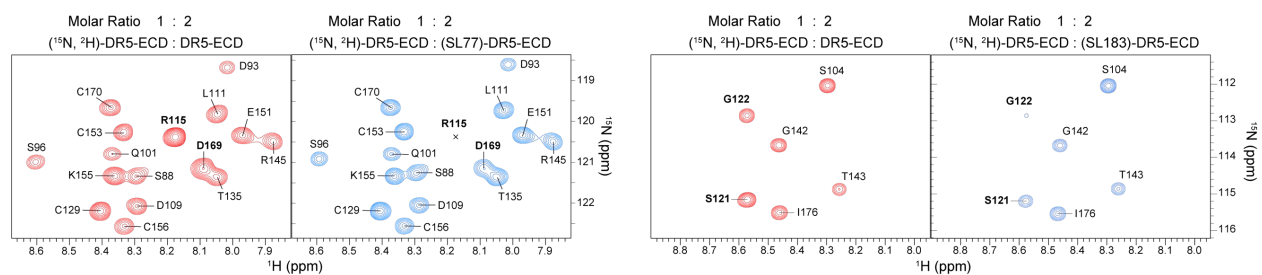
**b** Example NOE strips from 3D  $^{13}\text{C}$ -edited NOESY-HSQC spectra recorded with 28 ms  $^{13}\text{C}$  constant-time evolution and  $\tau_{\text{NOE}} = 150$  ms using an 0.4 mM ( $^{15}\text{N}$ ,  $^{13}\text{C}$ )-labeled DR5-ECD anchored to deuterated DMPC-DH<sub>7</sub>PC bicelles ( $q = 0.5$ ). The bicelle concentration was 0.8 mM, which corresponds to 4.4 mM DGS-NTA (Ni), 44 mM deuterated DMPC, and 88 mM deuterated DH<sub>7</sub>PC. The spectrum was recorded at 37°C and  $^1\text{H}$  frequency of 800MHz. Intermolecular NOEs are marked by green boxes.

**c** Ensemble of 15 lowest energy structures from 100 structures calculated using all NMR-derived restraints (intra- and inter- molecular). Protons are not displayed for clarity.

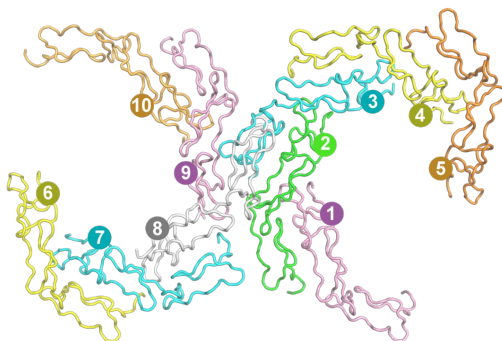
**d** Ribbon representation of the oligomeric structure showing intermolecular NOE restraints for the two non-overlapping interfaces as red lines.



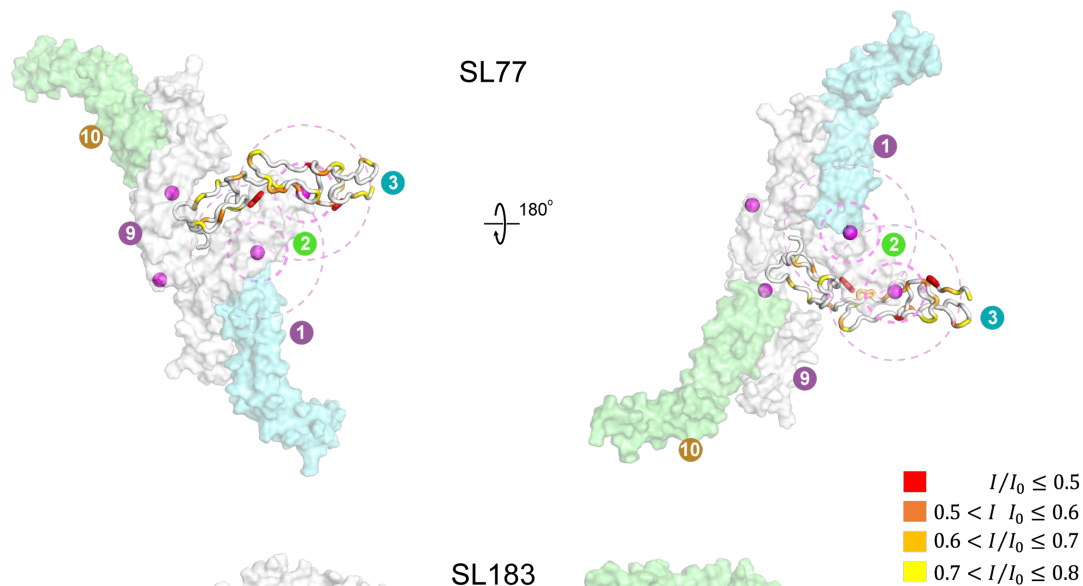
**a**



**b**



**c**



**d**

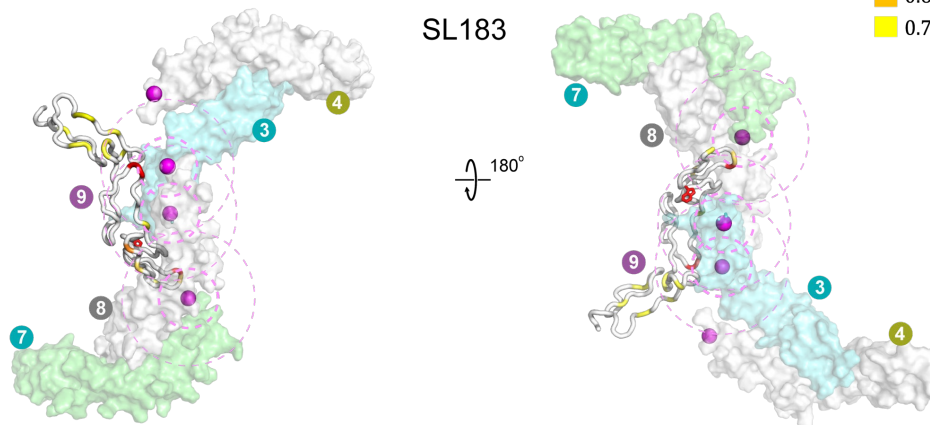


**Fig. S3: Analysis of DR5-ECD clustering on bicelle by the measurement of intermolecular PREs, related to Fig. 2**

**a** Sample regions of  $^1\text{H}$ - $^{15}\text{N}$  TROSY-HSQC spectra showing intermolecular PREs caused by spin label at residue 77 (upper panel) or 183 (lower panel). The spectra were recorded at 37°C and 700MHz using mixed samples comprising 100  $\mu\text{M}$  ( $^{15}\text{N}$ ,  $^2\text{H}$ )-labeled ECD for NMR readout and 200  $\mu\text{M}$  regular ECD with nitroxide label at residue 77 or 183 (blue spectra), all anchored to bicelles with  $q = 0.5$ . The reference spectra could not be obtained by reducing the nitroxide with 10 mM ascorbic acid as it also reduced some of the native disulfide bonds. Therefore, the reference spectra were recorded using a sample comprising 100  $\mu\text{M}$  ( $^{15}\text{N}$ ,  $^2\text{H}$ )-labeled ECD and 200  $\mu\text{M}$  regular ECD under identical condition (red spectra). Residues exhibiting significant intermolecular PRE are labeled in bold font.

**b** The possible higher-order cluster in Fig. 2e formed with interaction Interfaces 1 and 2 with defined protomer numbers.

**c-d** Mapping of intermolecular PREs onto the DR5-ECD structure. The monomer displaying intermolecular PREs is in cartoon tube representation and other monomers are surface rendered for clarity. The  $\text{C}_\beta$  atom of the spin-labeled residue of each of the surface-rendered monomers is highlighted in magenta sphere. PRE was calculated as the ratio of peak intensity of ( $^{15}\text{N}$ ,  $^2\text{H}$ )-labeled DR5-ECD mixed with spin-labeled DR5-ECD ( $I$ ) to that of ( $^{15}\text{N}$ ,  $^2\text{H}$ )-labeled DR5-ECD mixed with unlabeled DR5-ECD ( $I_0$ ). Stronger PRE means smaller value of ( $I/I_0$ ).

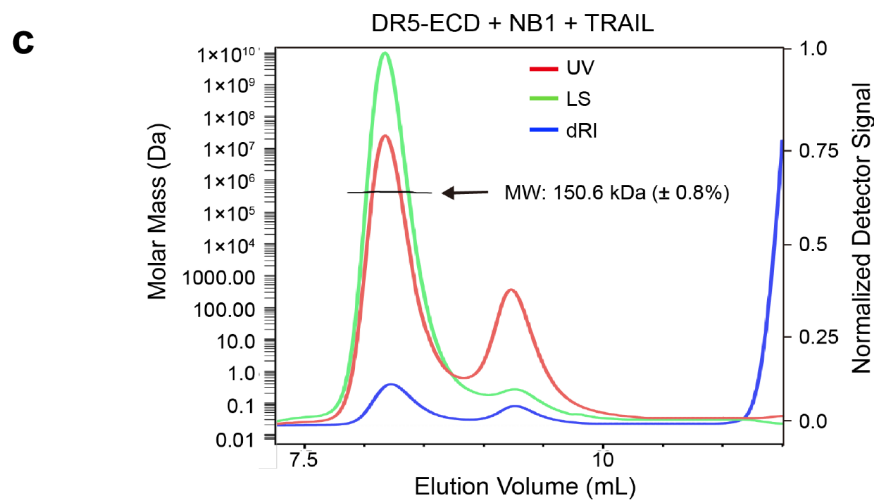
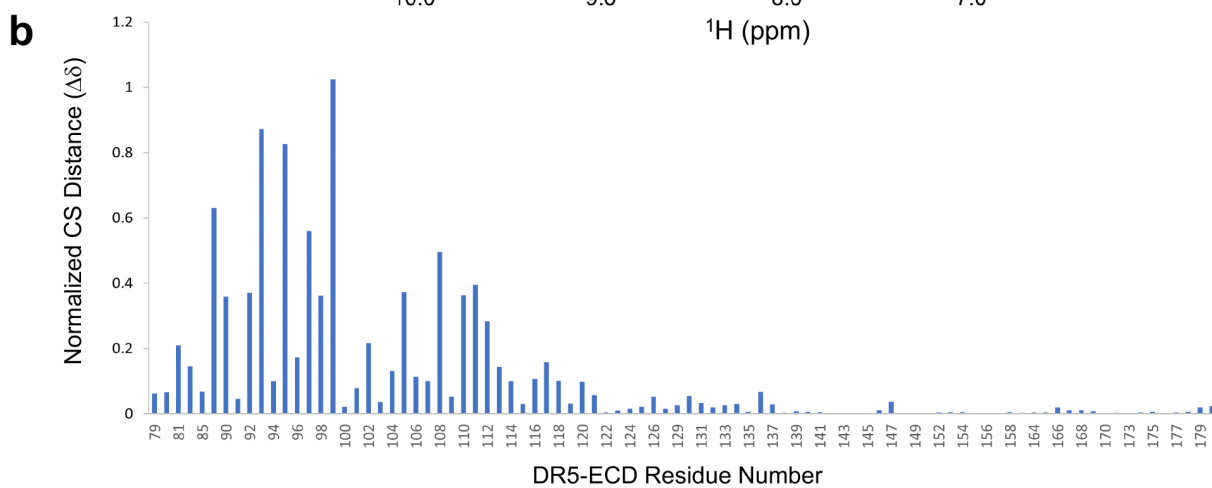
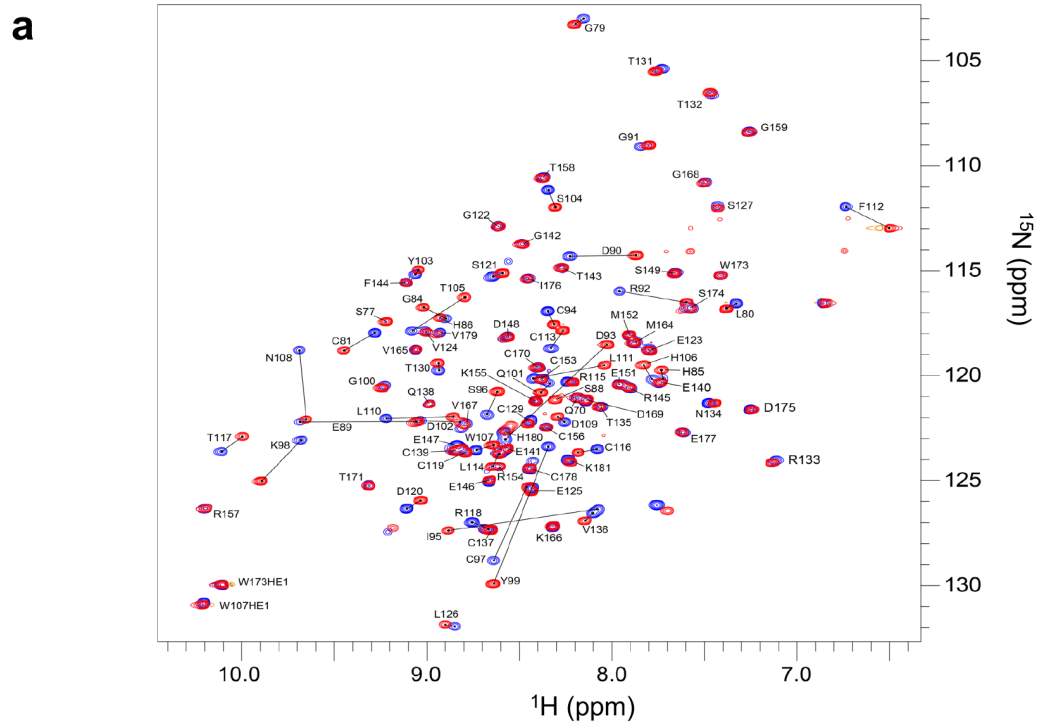


**Fig. S4: Epitope mapping of sdAb binding to DR5-ECD, related to Fig. 4**

**a** Overlay of  $^1\text{H}$ - $^{15}\text{N}$  TROSY-HSQC spectra of ( $^{15}\text{N}$ ,  $^{13}\text{C}$ , 85%  $^2\text{H}$ )-labeled DR5-ECD in the absence (red) and presence of 1:1 ratio of unlabeled NB1 (blue), recorded at 30°C and  $^1\text{H}$  frequency of 700MHz. The black lines indicate movement of DR5-ECD resonances upon binding to NB1.

**b** Normalized Chemical Shift Distance ( $\Delta\delta$ ) vs. Residue Number, showing that the largest perturbation by NB1 binding are in the CRD1 of DR5-ECD.  $\Delta\delta_{\text{RAW}} = [(\Delta\delta_{\text{H}})^2 + 0.15(\Delta\delta_{\text{N}})^2]^{1/2}$ ;  $\Delta\delta = \Delta\delta_{\text{RAW}} / \text{Max}(\Delta\delta_{\text{RAW}})$ .

**c** SEC-MALS analysis of DR5-ECD in complex with NB1 and the trimeric TRAIL. Chromatogram shows the readings from the LS (green), RI (blue), and UV (red) detectors. The left and right axes represent the molecular mass and normalized detector signal, respectively. The black line represents the calculated molecular mass from MALS and UV/RI. The average mass of the major elution peak is 150.6 kDa ( $\pm 0.8\%$ ), which is consistent with the sum of the theoretical molecular mass (147.9 kDa) of 3 x DR5-ECD (3 x 15.5 kDa), 3 x NB1 (3 x 14.3 kDa), and the trimeric TRAIL (58.5 kDa).



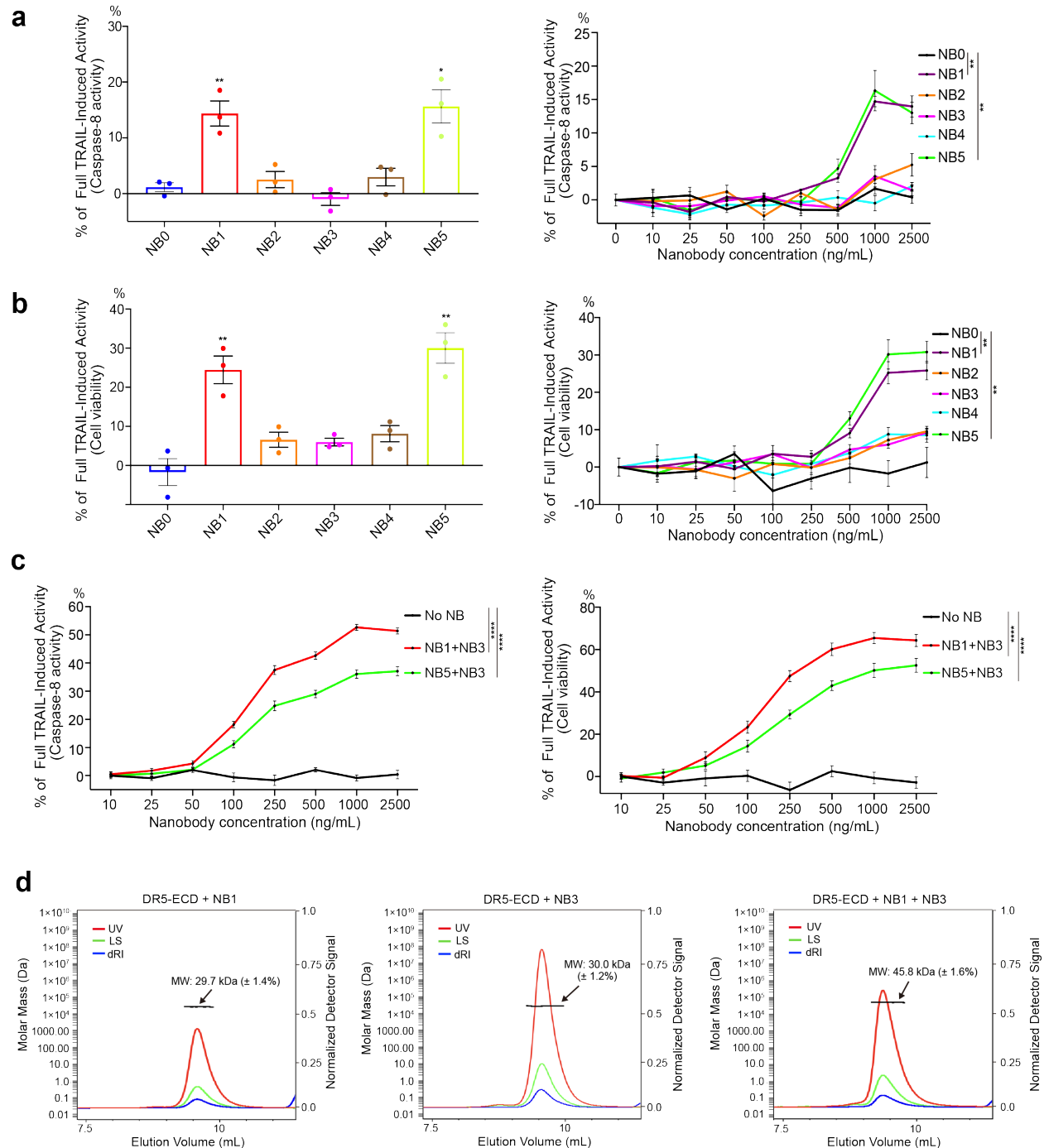


**Fig. S5: Agonistic effect of single and duo sdAbs in the absence of TRAIL and SEC-MALS analysis of binding, related to Fig. 5**

**a** Effect of the five individual sdAbs on DR5 signaling as reported by caspase-8 activity. Left and right panels report single dose (1  $\mu\text{g/mL}$ ) and dose-dependent DR5 activity, respectively. Monoclonal HEK293T stable cells expressing WT DR5 were treated with sdAbs for 6h. Caspase-

8 activity was measured using the CaspGLOW red caspase-8 activity kit and normalized as % of the fully saturated DR5 activation by TRAIL, indicated by  $\Delta 1$  in Fig. 4b. Results were obtained from 3 independent experiments ( $n = 3$ ) and expressed as mean  $\pm$  SEM. Error bars represent SEMs. Left: Student's t tests,  $*p < 0.05$ ,  $**p < 0.01$ . Right: two-way ANOVA,  $**p < 0.01$ .

**b** Same as in (a) using cell viability as readout. HEK293T stable cells expressing WT DR5 were treated with sdAbs for 12h. The reported activity is normalized as % of the fully saturated DR5 activation by TRAIL, indicated by  $\Delta 2$  in Fig. 4b. Error bars represent SEMs. Left: Student's t tests,  $**p < 0.01$ . Right: two-way ANOVA,  $**p < 0.01$ .

**c** Effect of combinations (NB1, NB3) and (NB5, NB3) on DR5 signaling in a dose-dependent manner, as reported by caspase-8 activity (left) and cell viability (right). The sdAb concentration values on the X-axes refer to the concentration of each sdAb in a combination. Error bars represent SEMs. Two-way ANOVA,  $****p < 0.0001$ .

**d** SEC-MALS analysis of DR5-ECD in complex with NB1, NB3, or NB1 + NB3. Chromatograms show the readings from the LS (green), RI (blue), and UV (red) detectors. The left and right axes represent the molecular mass and normalized detector signal, respectively. The black lines represent the calculated molecular mass from MALS and UV/RI. The average mass of the elution peak is 29.7 kDa ( $\pm 1.4\%$ ) for DR5-ECD bound to NB1, 30.0 kDa ( $\pm 1.2\%$ ) for DR5-ECD bound to NB3, and 45.8 kDa ( $\pm 1.6\%$ ) for DR5-ECD bound to NB1 and NB3, which are consistent with the sum of the theoretical molecular mass 29.8, 29.6, and 43.9 kDa, respectively.

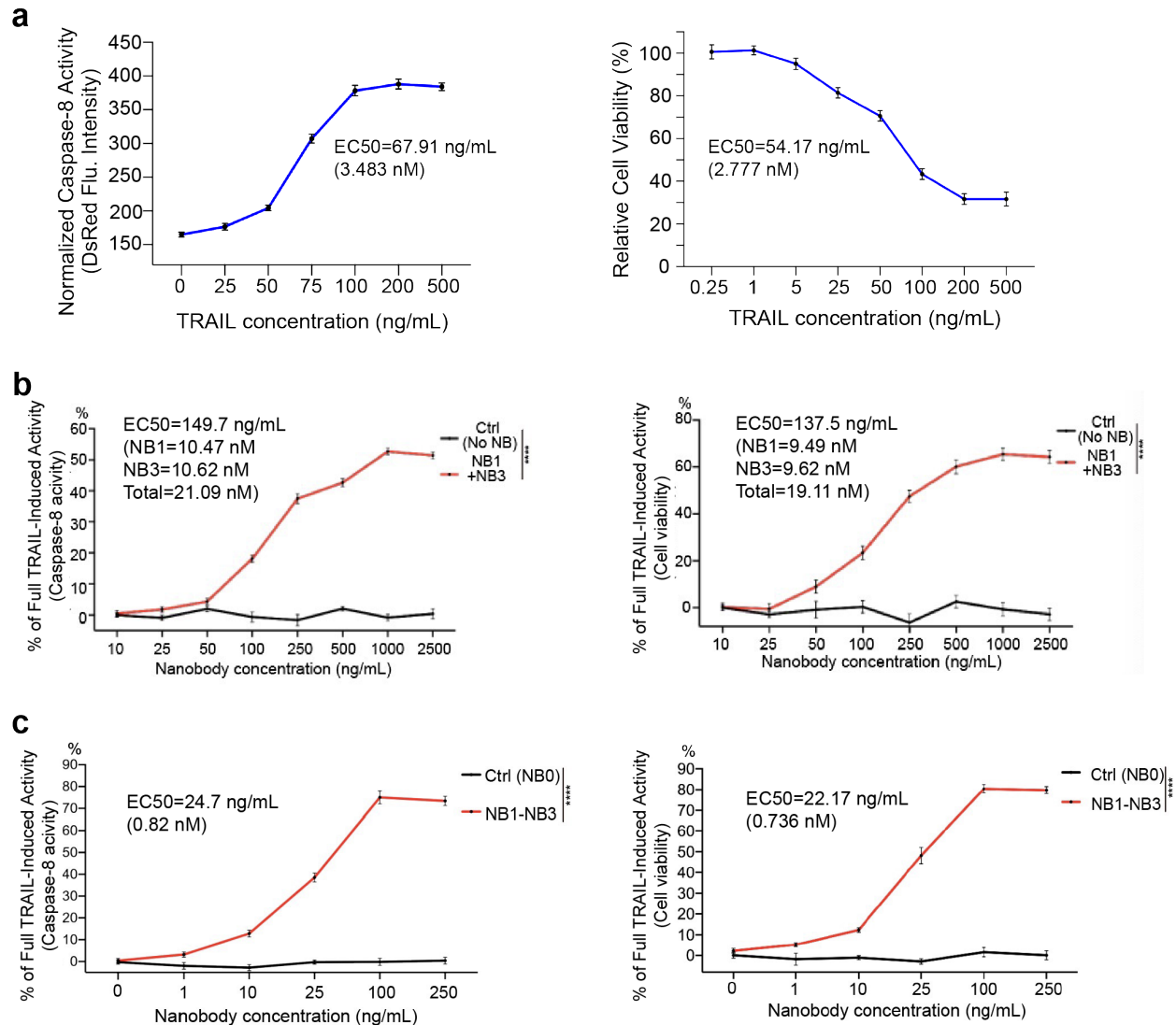


**Fig. S6: Covalently linking NB1 and NB3 drastically enhanced agonistic effect of the sdAbs in the absence of TRAIL, related to Fig. 5**

**a** TRAIL dose-response activation profiles based on caspase-8 activity (left) and cell viability (right). Data are from Fig. 4b. Calculated EC<sub>50</sub> are in TRAIL monomer concentration.

**b** Effect of combinations (NB1, NB3) on DR5 signaling in a dose-dependent manner, as reported by caspase-8 activity (left) and cell viability (right). Data are from Fig. S5c. Calculated EC<sub>50</sub> are in combined concentration of NB1 and NB3.

**c** Effect of covalently linking NB1 and NB3 (NB1-NB3) with 6 x GGGGS linker on DR5 signaling in a dose-dependent manner, as reported by caspase-8 activity (left) and cell viability (right). Error bars represent SEMs. Two-way ANOVA, \*\*\*\*p < 0.0001.



**Fig. S7: Schematic illustrations of the various Split-GFP constructs used for the analyses of DR5 self-association on the cell surface, related to Fig. 6**

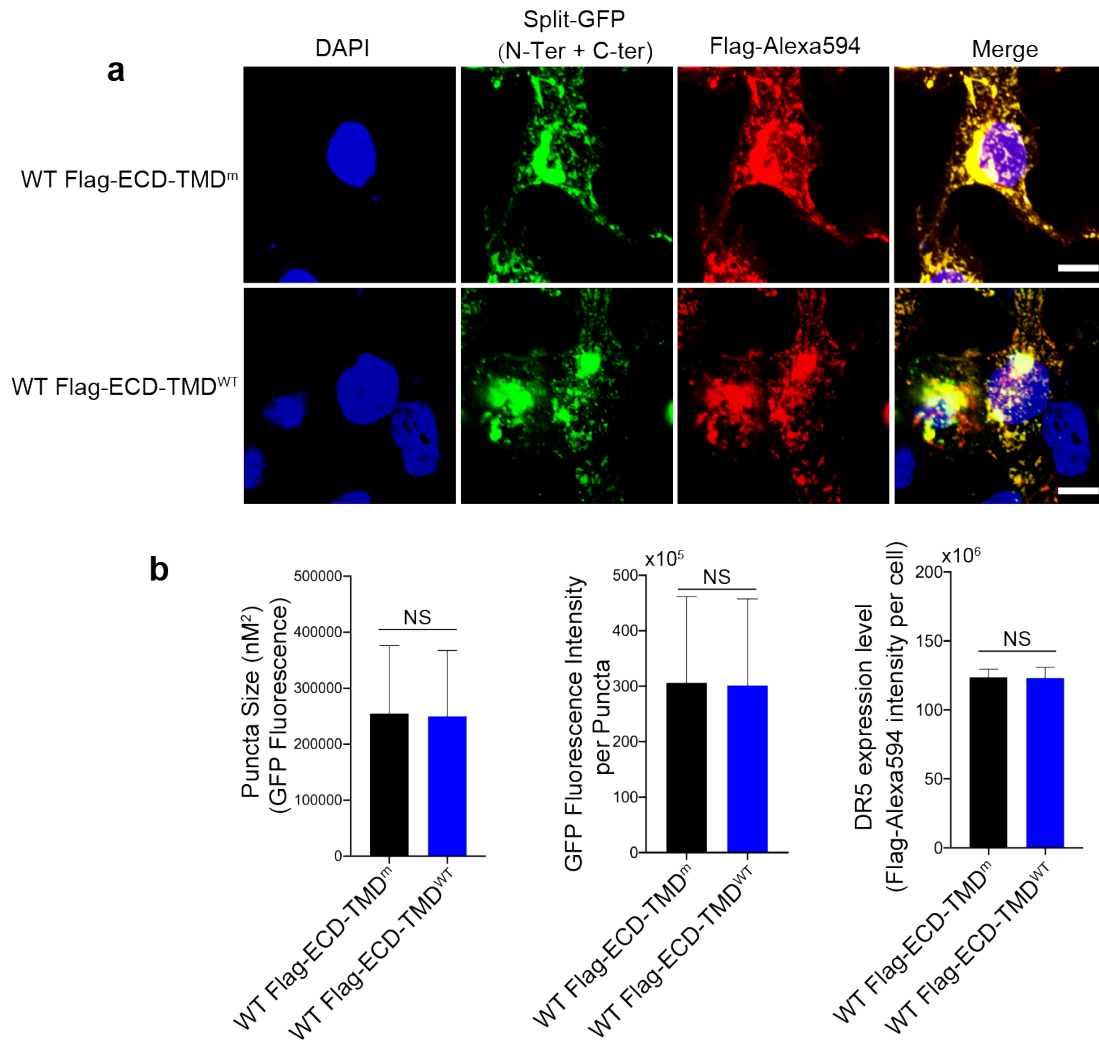


**Fig. S8. Comparison of preligand clustering and expression level between the ECD-TMD constructs with and without TMD mutations, related to Fig. 6**

**a** Confocal images of DR5 ECD-TMD<sup>m</sup> and DR5 ECD-TMD<sup>WT</sup> expressed in HEK293T cells. The constructs tested include the Flag-ECD-TMD<sup>m</sup>-GFP<sup>N/C</sup> (upper row) and Flag-ECD-TMD<sup>WT</sup>-GFP<sup>N/C</sup> (lower row). Cells were fixed with 4% paraformaldehyde and were then stained with Alexa Fluor® 594 anti-Flag antibody for 2h before imaging (405, 488 and 559 nm lasers were used for DAPI, split-GFP and Alexa549 channels, respectively). Images were taken with the Olympus Fluoview FV1000 confocal microscope. Scale bar, 5  $\mu$ m.

**b** Quantification of the size (left) and intensity (middle) of the puncta (or clusters) from GFP, and quantification of the expression levels (right) as reported by Flag-Alexa594 intensity using the Fiji software.



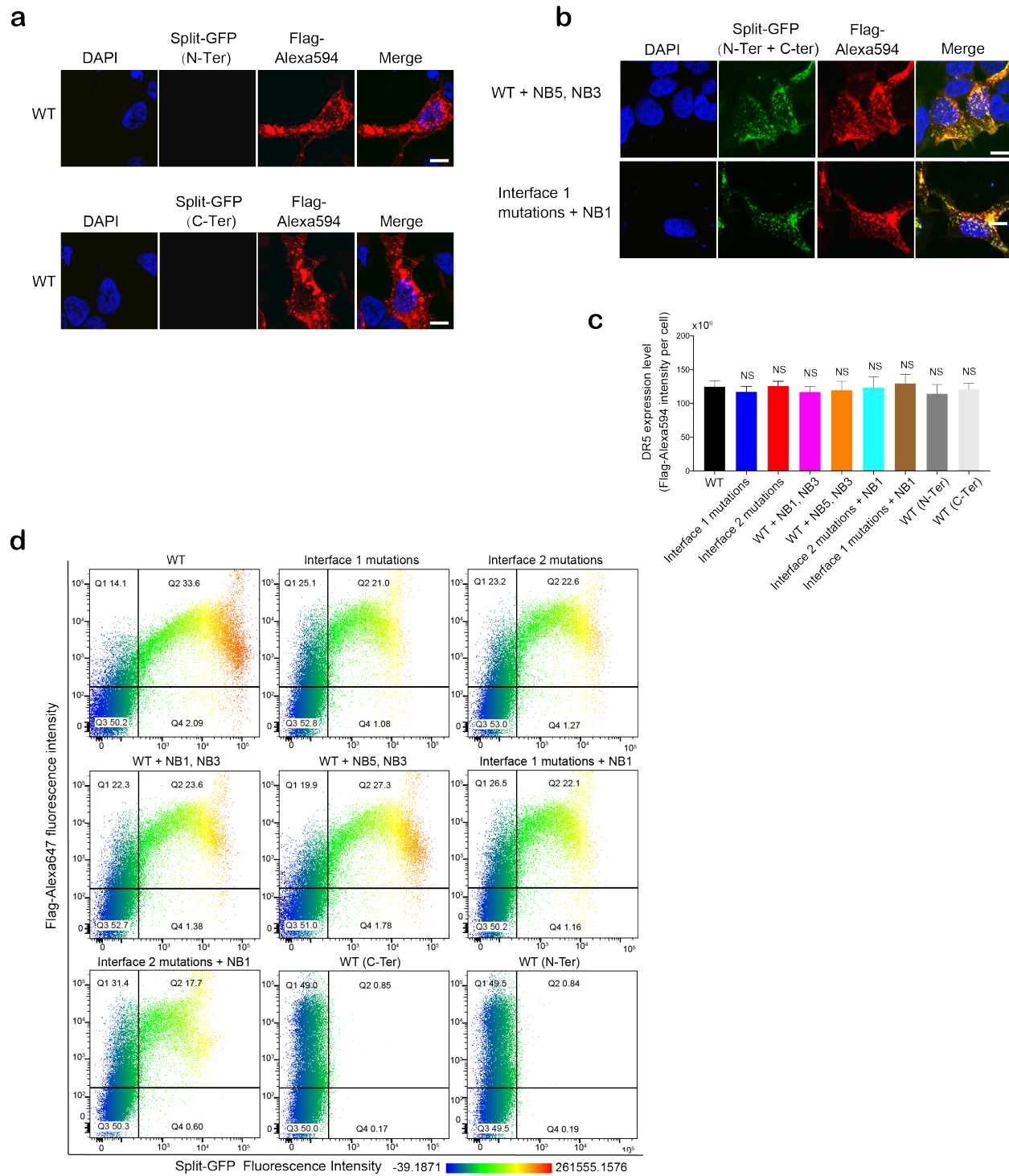


**Fig. S9: Additional confocal imaging and flow-cytometry analysis of DR5-ECD preligand association on cell surface, related to Fig. 6**

**a** Confocal images of WT Flag-ECD-TMD<sup>m</sup>-GFP<sup>N</sup> or Flag-ECD-TMD<sup>m</sup>-GFP<sup>C</sup> expressed separately as negative control. Images were taken with the Olympus Fluoview FV1000 confocal microscope. Scale bar, 5  $\mu$ m.

**b** Confocal images of WT Flag-ECD-TMD<sup>m</sup>-GFP<sup>N/C</sup> co-expressed in the presence of NB5 (1  $\mu$ g/mL) and NB3 (1  $\mu$ g/mL) (top) and of Flag-ECD-TMD<sup>m</sup>-GFP<sup>N/C</sup> with Interface 2 mutations co-expressed in the presence of NB1 (1  $\mu$ g/mL) on the HEK293T cell surface. Experimental conditions and analyses were the same as in Fig. 6a. Images were taken with the Olympus Fluoview FV1000 confocal microscope. Scale bar, 5  $\mu$ m.

**c** Quantification of the expression levels of Flag-ECD-TMD<sup>m</sup>-GFP<sup>N/C</sup> and variants in HEK293T cell as reported by Flag-Alexa594 intensity. The fluorescence intensity was integrated over each cell and averaged over 200 cells. Error bars represent SEMs. Student's t tests, NS (non-significant) represents  $p > 0.05$ .

**d** 2D flow-cytometry plots of both GFP (X-axis) and Flag-Alexa647 (Y-axis) fluorescence of Flag-ECD-TMD<sup>m</sup>-GFP<sup>N/C</sup> and variants expressed in HEK293T cells. WT or mutant Flag-ECD-TMD<sup>m</sup>-GFP<sup>N</sup> (400 ng) and Flag-ECD-TMD<sup>m</sup>-GFP<sup>C</sup> (386.4 ng) constructs were co-transfected at 1:1 molar ratio into HEK293T cells. 18h post-transfection, cells were stained with Alexa Fluor® 647 and analyzed by flow cytometry. The 633 nm laser with 670/20 band pass (BP) emission filter was used for Alexa Fluor® 647. The 488 nm laser was used to excite the split-GFP and measured with a 550/10 BP filter.

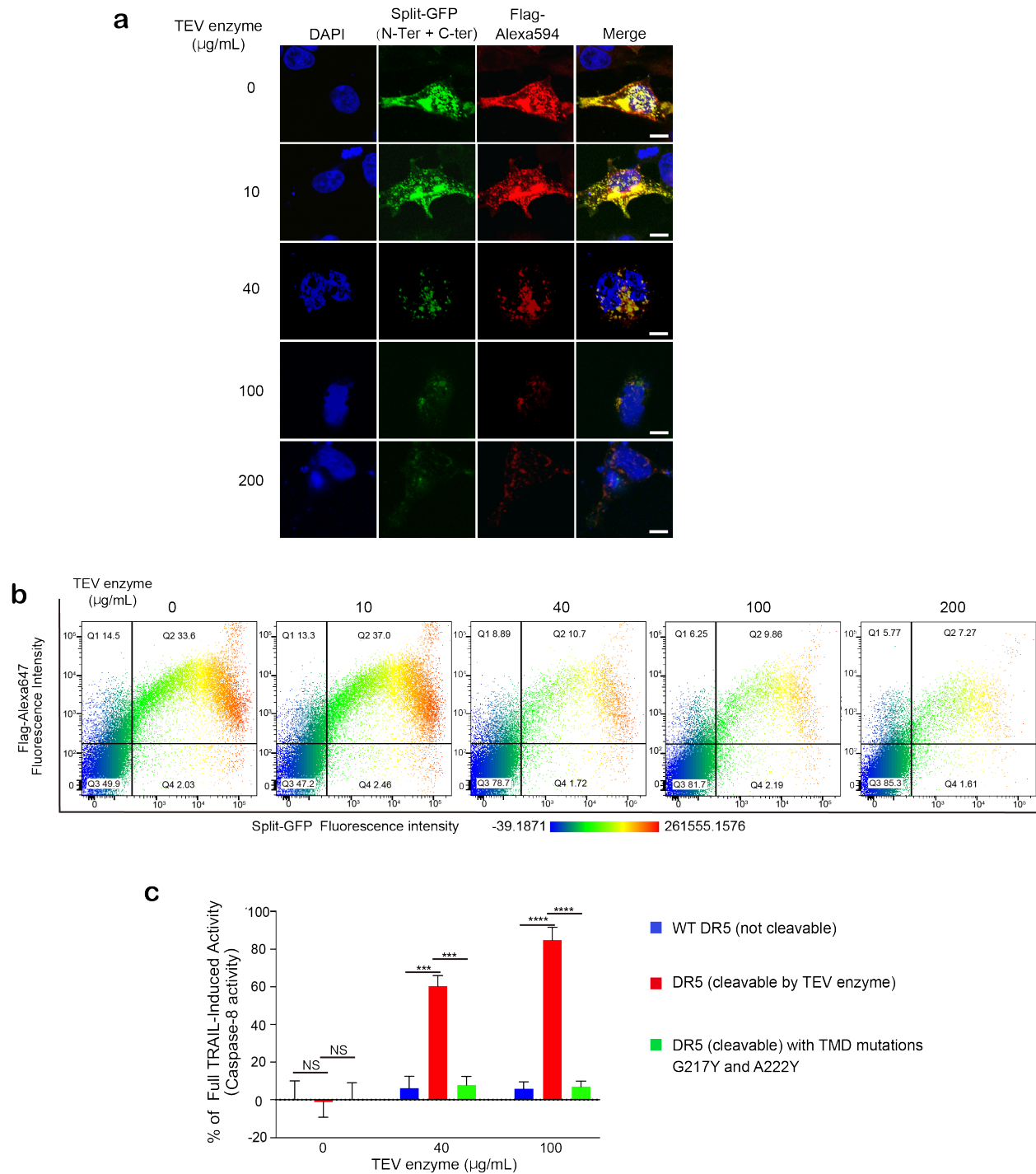


**Fig. S10: Additional characterization of the cleavable ECD-tev-TMD<sup>m</sup>-GFP<sup>N/C</sup> construct, related to Figs. 6 and 7**

**a** Confocal images of WT Flag-ECD-tev-TMD<sup>m</sup>-GFP<sup>N/C</sup> in HEK293T cells in the presence of TEV enzyme (0-200 μg/mL; for dose-dependent removal of the ECD), showing concomitant reduction of GFP fluorescence (TMD<sup>m</sup>-GFP<sup>N</sup> and TMD<sup>m</sup>-GFP<sup>C</sup> do not associate without ECD) and Alexa594

fluorescence (Flag-ECD shedding) as the TEV enzyme concentration increased. Images were taken with the Olympus Fluoview FV1000 confocal microscope. Scale bar, 5  $\mu$ m.

**b** 2D flow-cytometry plots of both GFP (X-axis) and Flag-Alexa647 (Y-axis) fluorescence of Flag-ECD-tev-TMD<sup>m</sup>-GFP<sup>N/C</sup> expressed in HEK293T cells in the presence of increasing concentrations of TEV enzyme.

**c** Comparing the functional effects of TEV enzyme on three DR5 constructs including the WT DR5 (not cleavable), the cleavable DR5 (TEV site between the ECD and TMD), and the cleavable DR5 with TMD mutations G217Y and A222Y that break TMD oligomerization. HEK293T cells were transiently transfected with the above three constructs. After transfection, cells were treated with TEV enzyme for 18h before analysis. Error bars represent SEMs. Student's t tests, \*\*\*p < 0.001, \*\*\*\*p < 0.0001, and NS (non-significant) represents p > 0.05.



**Table S1. NMR Structure Calculation and Refinement Statistics**

<b>NMR distance, dihedral and plane restraints <sup>a</sup></b>	<b>Interface 1</b>	<b>Interface 2</b>
Distance restraints from NOE	1414	
Short-range intramolecular ( $ i-j  \leq 4$ )	954	
Long-range intramolecular ( $ i-j  \geq 5$ )	399	
Intermolecular	37	24
Total dihedral angle restraints <sup>b</sup>	498	
$\Phi$ (TALOS)	249	
$\psi$ (TALOS)	249	
<b>Structure statistics <sup>c</sup></b>		
Violations (mean $\pm$ s.d.)		
Distance restraints ( $\text{\AA}$ )	0.072 $\pm$ 0.002	
Dihedral angle restraints ( $^\circ$ )	1.433 $\pm$ 0.050	
Deviations from idealized geometry		
Bond lengths ( $\text{\AA}$ )	0.006 $\pm$ 0.000	
Bond angles ( $^\circ$ )	0.775 $\pm$ 0.006	
Impropers ( $^\circ$ )	0.546 $\pm$ 0.010	
Average pairwise r.m.s. deviation ( $\text{\AA}$ ) <sup>d</sup>		
Heavy	0.464	
Backbone	1.045	

<sup>a</sup> The numbers of restraints are summed over all three subunits and over residues 79-179 of the DR5-ECD.

<sup>b</sup> Backbone  $\phi$  and  $\psi$  restraints and their respective uncertainties were obtained from the “GOOD” dihedrals generated by TALOS+ based on chemical shift values of backbone  $^1\text{H}^N$ ,  $^{15}\text{N}$ ,  $^{13}\text{C}'$ ,  $^{13}\text{C}^\alpha$ , and  $^{13}\text{C}^\beta$ .

<sup>c</sup> Statistics were calculated and averaged over an ensemble of the 15 lowest energy structures out of 100 calculated structures.

<sup>d</sup> The precision of the atomic coordinates is defined as the average r.m.s. difference between the 15 final structures and their mean coordinates.